



(Project Number: 945 041)

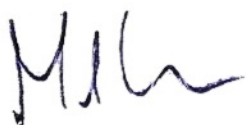
## DELIVERABLE D5.3

### Definition of the Thermal-Hydraulic Benchmark

Lead Beneficiary: CENTRUM VYZKUMU REZ

Due date: 31/01/2023

Released on: 10/02/2023

<b>Authors:</b>	Tomáš Melichar, Jan Šefl, Daniel Kříž	
<b>For the Lead Beneficiary</b>	<b>Reviewed by Work package Leader</b>	<b>Approved by Coordinator</b>
<b>Tomáš MELICHAR</b> 	<b>Eugene SHWAGERAUS</b> 	<b>Branislav HATALA</b> 

Start date of project:

**01/10/2020**

Duration: **48 Months**

Project Coordinator:

**Branislav Hatala**

Project Coordinator Organisation:

**VUJE, a. s.**

VERSION: **1.2**

<b>Project co-funded by the European Commission under the Euratom Research and Training Programme on Nuclear Energy within the Horizon 2020 Programme</b>		
<b>Dissemination Level</b>		
<b>PU</b>	Public	<b>X</b>
<b>RE</b>	Restricted to a group specified by the Beneficiaries of the MEET-CINCH project	
<b>CO</b>	Confidential, only for Beneficiaries of the MEET-CINCH project	

### Version control table

Version number	Date of issue	Author(s)	Brief description of changes made
1.0	31.01.2023	Tomas Melichar	
1.1	10.02.2023	Involved partners Michaela Velčková	Reviewed by consortium and partners involved in WP5 Reviewed by MST
1.2.	20.02.2023	Eugene SHWAGERAUS	Reviewed by WP leader Final version

### Project information

Project full title:	Safety of GFR through innovative materials, technologies and processes
Acronym:	SafeG
Funding scheme:	Research and innovation action
ECGA number:	945041
Programme and call	Horizon 2020 Framework Programme for Research and Innovation (2014-2020) NFRP-2019-2020 (Nuclear Fission and Radiation Protection Research)
Coordinator:	Dr. Branislav Hatala
EC Project Officer:	Dr. Cristina Fernandez Ramos
Start date – End date:	01/10/20 – 30/09/2024 i.e. 48 months
Coordinator contact:	+421 905 567 985, branislav.hatala@vuje.sk
Administrative contact:	+420 602 771 784, jakub.heller@evalion.cz
Online contacts (website):	<a href="http://www.safeg.eu">www.safeg.eu</a>

### Copyright

The document is proprietary of the SafeG consortium members. No copying or distributing, in any form or by any means, is allowed without the prior written agreement of the owner of the property rights. This document reflects only the authors' view. The European Community is not liable for any use that may be made of the information contained herein.



*„This project has received funding from the Euratom research and training programme 2019-2020 under grant agreement No 945041”.*

## EXECUTIVE SUMMARY

A thermal-hydraulic modelling benchmark is organized within the SafeG project. The benchmark is split in two parts, (1) CFD benchmark on (2) systemic codes benchmark on the S-Allegro facility. The purpose of this document is to describe the benchmarks in detail to allow the benchmarks participants to create computational models and carry out the required simulations. The description includes a description of the experimental facilities, geometry, operational parameters and selected experimental data needed for the codes benchmarking.

This document is prepared in compliance with the template provided by the Commission in Annex 1 of the Guidelines on Data Management in Horizon 2020.

## LIST OF ABBREVIATIONS

BME	Budapest University of Technology and Economics
CFD	Computational Fluid Dynamics
CVR	Centrum výzkumu Řež
I.C	Primary Circuit
II.C	Secondary Circuit
III.C	Tertiary Circuit
ID	Inner Diameter
OD	Outer Diameter
PHX	Primary Heat Exchanger
SHX	Secondary Heat Exchanger
STH	Systemic Thermal-hydraulic
RV	Reactor Vessel

## CONTENT

<b>1</b>	<b>INTRODUCTION .....</b>	<b>5</b>
<b>2</b>	<b>SYSEMIC CODES BENCHMARK ON S-ALLEGRO.....</b>	<b>6</b>
2.1	DESCRIPTION AND LAYOUT OF THE FACILITY .....	6
2.2	PIPELINE .....	9
2.3	REACTOR VESSEL .....	12
2.4	PRIMARY HEAT EXCHANGER .....	14
2.5	SECONDARY HEAT EXCHANGER .....	16
2.6	DHR HEAT EXCHANGER .....	18
2.7	COMPRESSORS.....	18
2.8	COAXIAL VALVES .....	20
2.9	TERTIARY CIRCUIT .....	21
2.10	OTHER SYSTEMS .....	21
2.11	INSTRUMENTATION .....	22
<b>3</b>	<b>DESCRIPTION OF EXPERIMENTS AND DATA FOR BENCHMARKING .....</b>	<b>26</b>
3.1	NOMINAL PARAMETERS .....	26
3.2	STEADY-STATE DATA ON HEAT EXCHANGERS.....	26
3.3	STEADY-STATE DATA – PRIMARY LOOPS OPERATION .....	27
3.4	TRANSIENT DATA .....	27
<b>4</b>	<b>CONCLUSION.....</b>	<b>28</b>
	<b>ATTACHMENT NR. 1 - ALLEGRO CFD BENCHMARK.....</b>	<b>29</b>
	<b>REFERENCES .....</b>	<b>41</b>

# 1 INTRODUCTION

---

The activity is split into two parts, (1) CFD benchmark on experiments on The PIROUETTE facility of BME and (2) systemic thermal-hydraulic codes (STH) on the experiments from the S-Allegro facility of CVR. In this document, both benchmarks are defined and described in order to allow the benchmark participants to prepare the numerical model. Therefore, the geometric and operational parameters as well as instrumentation for both facilities are described. The document is primarily intended for the benchmark participants as input documentation for the numerical models preparation.

Especially the part of the deliverable focused on the STH benchmark will be continuously updated. It is given due to current modifications of the S-Allegro facility and due to the fact that some parameters might be missing that might be however revealed during the models preparation phase. The experimental data will be also added in the next version of the deliverable as they are scheduled for 2023. To enhance the clarity of the benchmarks descriptions, the STH benchmark is described in this report and the CFD benchmark description is attached as a separate document.

The benchmark results will be evaluated in the following deliverable D5.4 – Results of the thermal-hydraulic benchmark. Comparison and assessment of the numerical results of the benchmark participants will be given. As the activity is ongoing within the “Education and benchmark” work package and the allocated personal resources in the project for this activity are limited, the purpose of the benchmark is rather educational and collecting of inputs for possible further, more detailed benchmarks.

## 2 SYSEMIC CODES BENCHMARK ON S-ALLEGRO

In this part, the S-Allegro facility is described from the geometric and operational parameters point of view to allow the benchmark participants to prepare the numerical models using STH codes. Geometric parameters, operational characteristics, locations and types of selected instrumentation is given below.

### 2.1 Description and layout of the facility

S-Allegro is a large-scale experimental facility operated by CVR in Pilsen, Czech Republic. The purpose of the facility is to support the development of the GFR demonstrator ALLEGRO. For this reason, S-Allegro is designed as an electrically heated scale-down of ALLEGRO so the layout of the main loops and the components is similar to expected in the GFR reactor. The heating power of S-Allegro is approx. 1 MW (1/75 scale-down compared to the ALLEGRO power). The main purpose of the facility is thermal-hydraulic verification of the high-temperature helium system during various operational conditions including accidental ones and the production of data for the numerical codes validation. The layout of the facility is shown in Figure 2-1. It is composed of the primary helium circuit (I.C) with the reactor vessel (RV), secondary helium circuit (II.C), tertiary water circuit (III.C) and DHR circuit that is also connected to the RV.

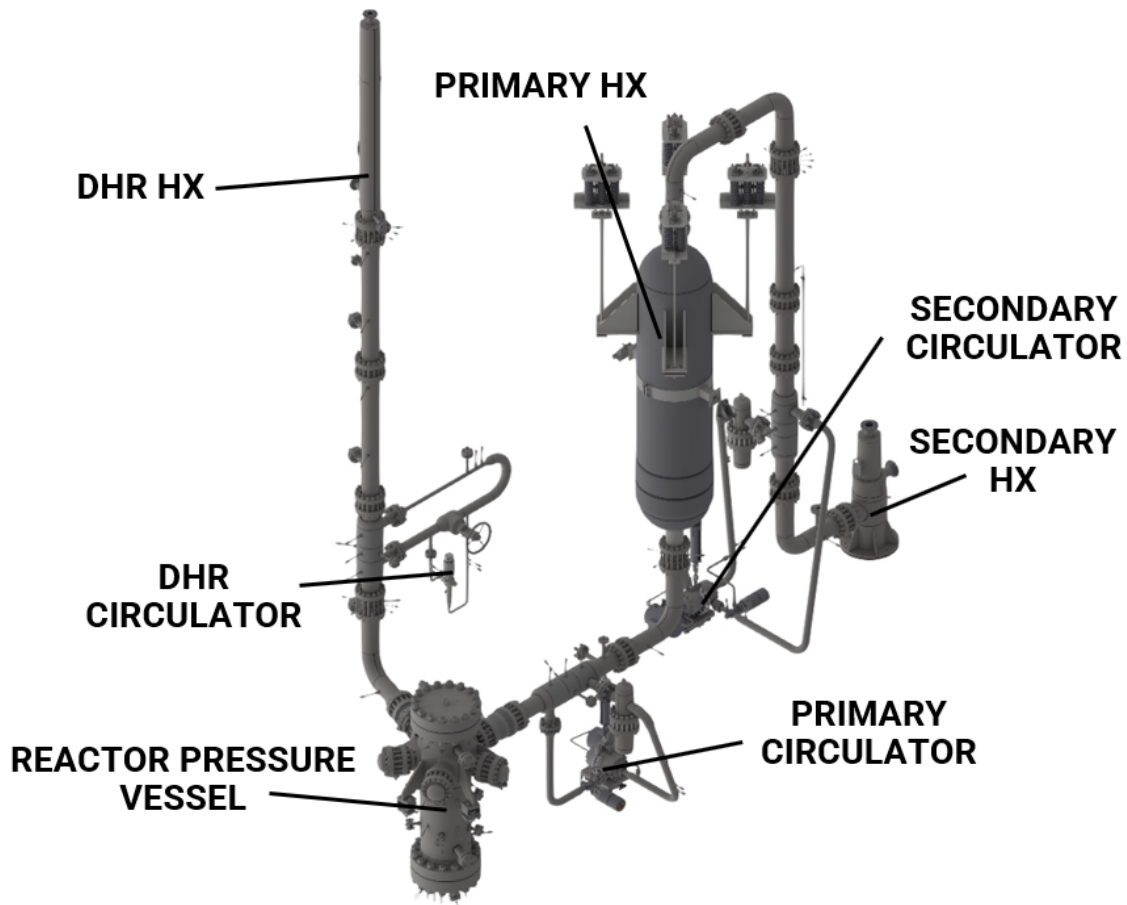


Figure 2-1: Layout of the S-Allegro facility

The process diagram is shown in Figure 2-2.

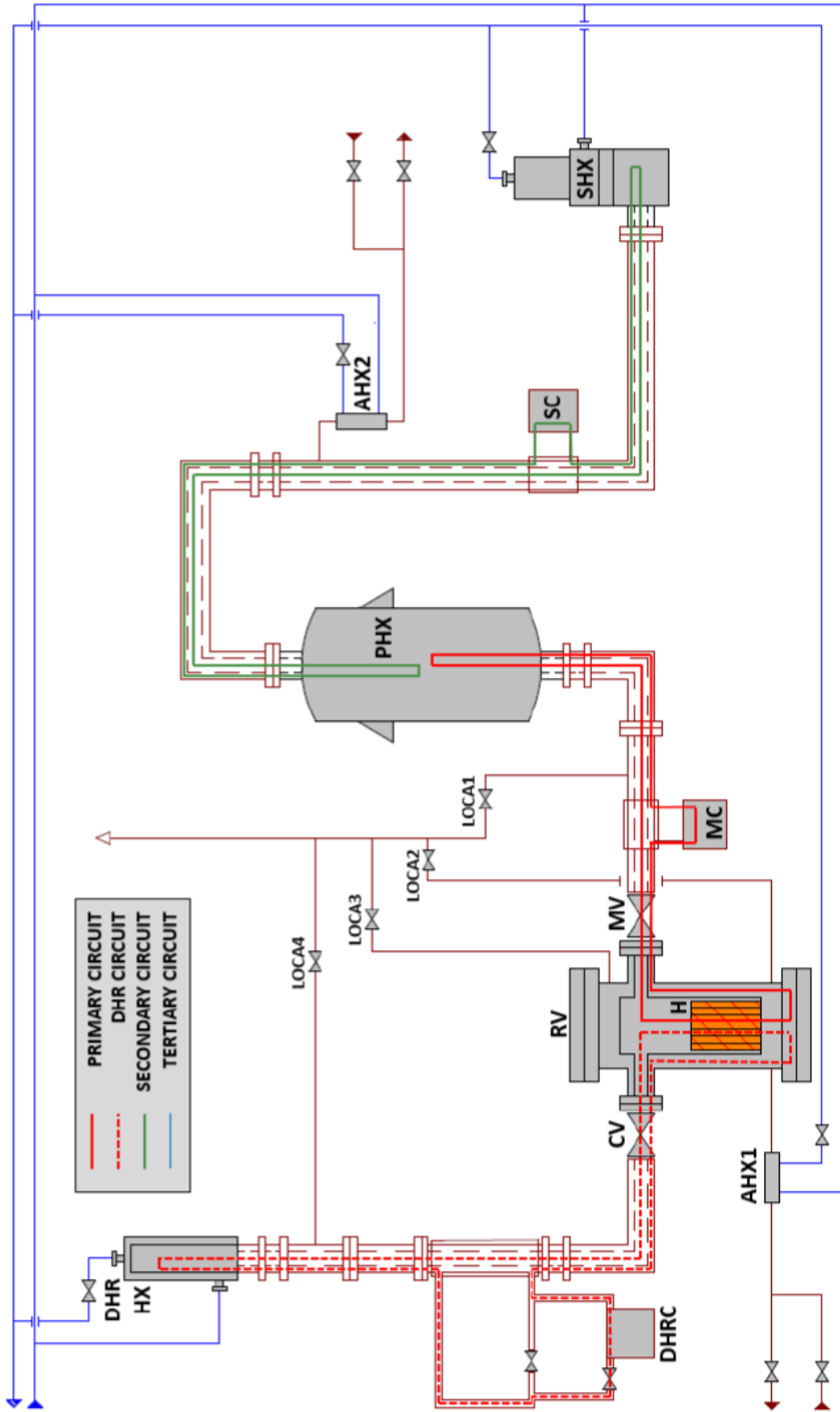


Figure 2-2: Scheme of the S-Allegro facility

In Figure 2-2, the RV is the reactor vessel, H is the heating section, DHR HX is the DHR heat exchanger, PHX is the primary HX, SHX is the secondary HX, DHRC is DHR circulator, MC is the main circulator, SC is the secondary circulator, AHX1-2 are the auxiliary HXs, CV is the DHR cross valve, MV is the main coaxial valve and LOCA1-4 are the LOCA valves.

The I.C contains the RV equipped with an electrical heating system. Forced convection in the I.C is ensured by a primary circulator. Moreover, a dedicated DHR circuit intended for the heat removal from the RV by natural or combined helium convection is connected to the I.C. During the nominal operation, the heat from the I.C is transferred to the II.C with forced circulating helium through a primary heat exchanger (PHX). The purpose of the III.C is the heat removal from both the I.C (through the DHR HX) and the II.C through the secondary HX (SHX).

After discharge of the PC, the primary helium flows (flow rate of up to 0.5 kg/s) through the outer part of a primary coaxial pipeline and enters the RV. In the RV, the helium first flows through a downcomer. In the bottom part of the RV, it turns 180° and enters the heating section representing active core of the GFR reactor. The core is composed of seven hexagonal heating assemblies; each assembly contains 18 ceramic channels. In each channel, a helical resistive heating wire is inserted. The total heating power of the core is 1 MW. After the RV, the helium of up to 900°C is flowing through the internal part of the coaxial pipeline in the primary HX and then through a filtering system in the suction of the PC. The maximum operating pressure in the I.C is 7 MPa.

The DHR circuit is connected to the RV and is therefore interconnected with the primary circuit. The DRH circuit is intended for the removal of the decay heat from the active core of the GFR reactor, in the case of S-Allegro from the RV. The electrical heaters are controllable to allow simulation of the real decay heat development. During normal operation of the DHR circuit, the primary circuit is closed and the helium flows only through the RV and the primary circuit. The DHR circuit is vertically oriented with a height of approx. 12.5 m to enhance the effect of the natural convection. The DHR circuit is also equipped with a circulator to allow combined convection. At the top part of the DHR circuit, a DHR HX is located where the heat from the helium is removed by the tertiary water circuit.

The primary circuit contains two special valves ensuring the required operational regimes, which were designed by CVR. The main valve is located on the primary pipeline between the RV and the main circulator. The function of this component is to shut off the primary circuit during the DHR operation. The second valve, so called “cross-valve”, is located on the DHR circuit. During the nominal operation of the primary circuit, the cross-valve is in the closed state but a small part of the flow-rate is allowed to pass through the DHR circuit in order to preheat the DHR section and to facilitate the establishment of the natural convection. The cross-valve opens at the same time when the primary valve is closed and then, the normal flow through the DHR loop is ensured.

The II.C removes the heat from the I.C. The heat is transferred in the primary HX. The forced circulation is given by the secondary circulator ensuring a flow rate up to 0.45 kg/s. The maximum operational pressure of the II.C is 6.5 MPa. The layout of the II.C is relatively simple, the helium flows through the shell side of the PHX, the secondary circulator with a filtering system and the tube side of the SHX.

The III.C removes heat from both the helium circuits. The III.C is connected to an existing cooling system that is used also for other technologies in the experimental hall. The water temperature at the inlet to the secondary HX corresponds to the ambient temperature. The circuit is operated at a pressure up to 6 bar. The maximum water flow rate is 100 m<sup>3</sup>/hod.

Description of the individual components follows.

## 2.2 Pipeline

The helium pipelines of the I.C, II.C and DHR circuits are designed as coaxial pipes where the hot leg is inside the cold one. The heat transfer between the legs is reduced by thermal insulation between the internal and external tubes. The external surface of the pipelines as well as of the other components is covered by a layer of thermal insulation to reduce heat losses.

There is Promalight 1000X insulation layer between the inner and outer tube. There is also a cover tube (stainless steel, 3 mm wall thickness) on the outer surface of the inner insulation. Two layers of outer insulation (Fiberfrax Durablanket S160 inner, ProRox WM 950 ALU outer, 50 mm thickness each) are applied on the outer surface of the outer tube. Physical properties of the insulation materials are listed in Tab. 2-4, Tab. 2-5 and Tab. 2-6. The inner tube is made of austenitic steel 301, the outer tube is made of steel 321.

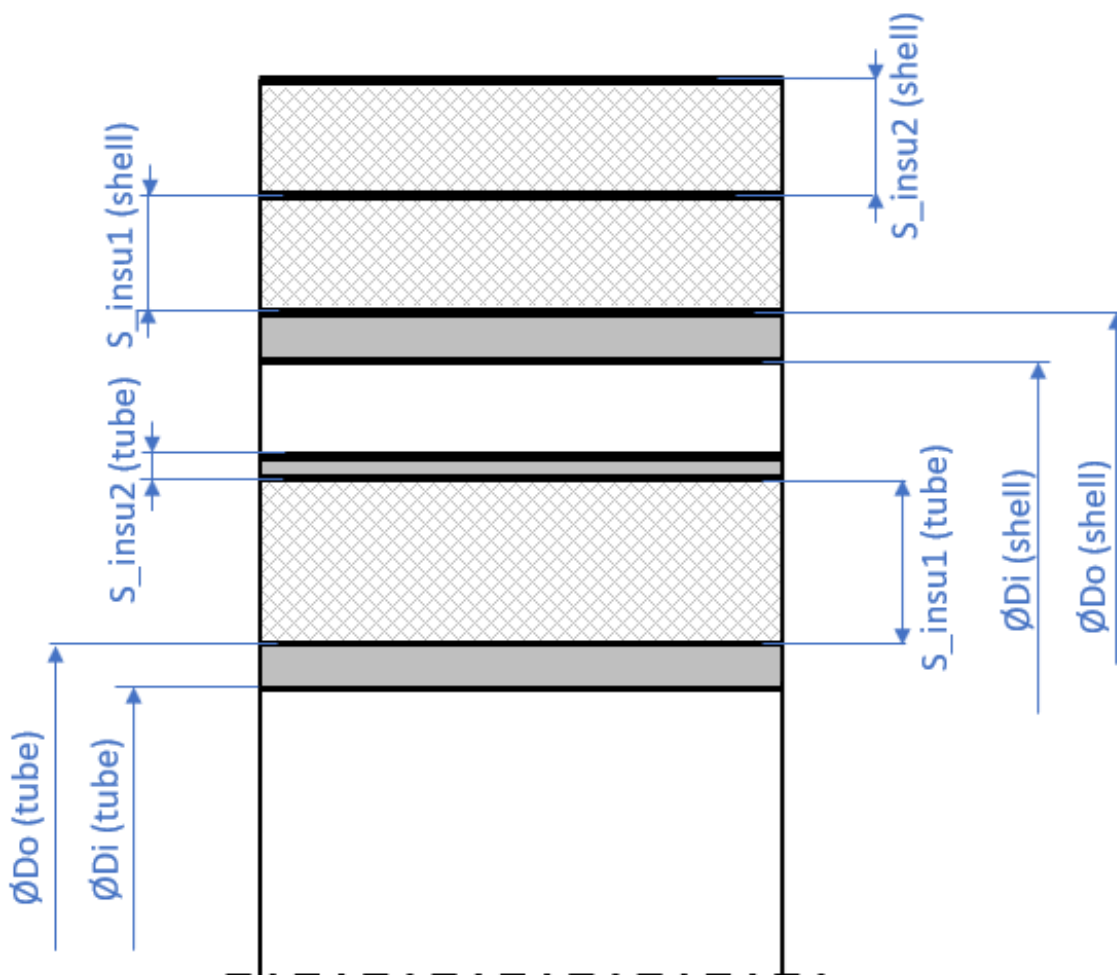


Figure 2-3: Coaxial tubes scheme

The dimensions of the pipeline are summarized for all circuits in Tab. 2-1, Tab. 2-2 and Tab. 2-3. The layout of the pipeline is then shown in Figure 2-4.

**Tab. 2-1: Dimensions of pipelines of the primary circuit**

	Primary circuit		Do		L [m]	s_insul [m]	s_insu2 [m]	z_in [m]	z_out [m]
			Di [m]	[m]					
<b>B</b>	Behind_Compressor	Shell	0.1937	0.2191	1.45	0.05	0.05	2.81	2.81
<b>A</b>	Reactor_FlangeOUT	Shell	0.1937	0.2191	0.25	0.05	0.05	2.81	2.81
<b>A</b>	Reactor_FlangeIN	Tube	0.0902	0.1016	0.25	0.03035	0.003	2.81	2.81
<b>B</b>	Behind_Valve	Tube	0.0902	0.1016	1.45	0.03035	0.003	2.81	2.81
<b>C</b>	In_Front_of_Bend	Tube	0.0902	0.1016	1.86	0.03035	0.003	2.81	2.81
<b>D</b>	In_Front_of_HE1	Tube	0.0902	0.1016	2.105	0.03035	0.003	2.81	4.915
<b>D</b>	Behind_HE1	Shell	0.1937	0.2191	2.105	0.05	0.05	4.915	2.81
<b>C</b>	In_Front_of_Compressor	Shell	0.1937	0.2191	1.86	0.05	0.05	2.81	2.81

**Tab. 2-2: Dimensions of pipelines of the secondary circuit**

	Secondary circuit		Do		L [m]	s_insul [m]	s_insu2 [m]	z_in [m]	z_out [m]
			Di [m]	[m]					
<b>E</b>	Behind_Compressor2	Shell	0.1937	0.2191	4.025	0.05	0.05	4.84	8.865
<b>D</b>	In_Front_of_BendOUT	Shell	0.1937	0.2191	0.875	0.05	0.05	8.865	9.73
<b>C</b>	BetweenOUT_Bends	Shell	0.1937	0.2191	1.9	0.05	0.05	9.73	9.73
<b>B</b>	In_Front_of_HE1_Secondary	Shell	0.1937	0.2191	0.875	0.05	0.05	9.73	8.865
<b>A</b>	HE1_FlangeOUT_Secondary	Shell	0.1937	0.2191	1.16	0.05	0.05	8.865	7.715
<b>A</b>	HE1_FlangeIN_Secondary	Tube	0.0902	0.1016	1.16	0.03035	0.003	7.715	8.865
<b>B</b>	In_Front_of_BendIN	Tube	0.0902	0.1016	0.875	0.03035	0.003	8.865	9.73
<b>C</b>	BetweenIN_Bends	Tube	0.0902	0.1016	1.9	0.03035	0.003	9.73	9.73
<b>D</b>	Behind_Bend	Tube	0.0902	0.1016	0.875	0.03035	0.003	9.73	8.865
<b>E</b>	Behind_Bend1	Tube	0.0902	0.1016	4.025	0.03035	0.003	8.865	4.84
<b>F</b>	In_Front_of_BendIN_HE2	Tube	0.0902	0.1016	1.93	0.03035	0.003	4.84	2.91
<b>G</b>	In_Front_of_HE2	Tube	0.0902	0.1016	1.07	0.03035	0.003	2.91	2.91
<b>G</b>	Behind_HE2	Shell	0.1937	0.2191	1.07	0.05	0.05	2.91	2.91
<b>F</b>	In_Front_of_Compressor2	Shell	0.1937	0.2191	1.93	0.05	0.05	2.91	4.84

**Tab. 2-3: Dimensions of pipelines of the DHR circuit**

	DHR		Do		L [m]	s_insul [m]	s_insu2 [m]	z_in [m]	z_out [m]
			Di [m]	[m]					
<b>H</b>									
<b>C</b>	Behind_Compressor_DHR	Shell	0.1937	0.2191	2.25	0.05	0.05	5.06	2.81
<b>B</b>	In_Front_of_Reactor_DHR	Shell	0.1937	0.2191	1.42	0.05	0.05	2.81	2.81
<b>A</b>	Reactor_FlangeOUT_DHR	Shell	0.1937	0.2191	0.25	0.05	0.05	2.81	2.81
<b>A</b>	Reactor_FlangeIN_DHR	Tube	0.0902	0.1016	0.25	0.03035	0.003	2.81	2.81
<b>B</b>	In_Front_of_Bend_DHR	Tube	0.0902	0.1016	1.42	0.03035	0.003	2.81	2.81
<b>C</b>	Behind_Bend_DHR	Tube	0.0902	0.1016	2.25	0.03035	0.003	2.81	5.06
<b>D</b>	In_Front_of_DHR	Tube	0.0902	0.1016	4.69	0.03035	0.003	5.06	9.75
<b>D</b>	Behind_DHR	Shell	0.1937	0.2191	4.69	0.05	0.05	9.75	5.06

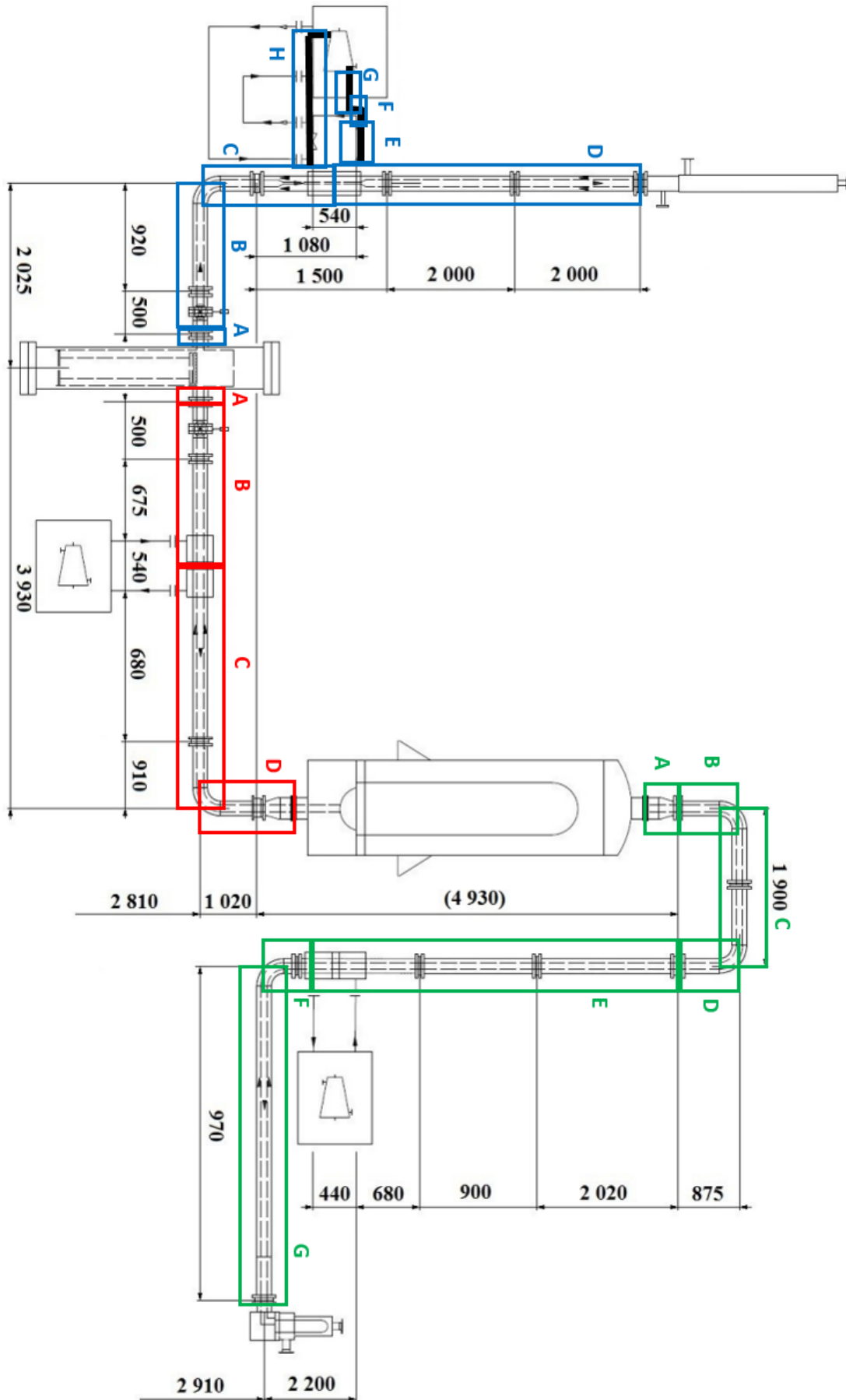


Figure 2-4: Pipeline layout and dimensions

**Tab. 2-4: Promalight 1000X insulation properties**

<b>Promalight 1000X</b>		
Density	280 kg/m <sup>3</sup>	
Thermal Conductivity	200 °C	0.023 W/mK
	400 °C	0.026 W/mK
	600 °C	0.030 W/mK
	800 °C	0.036 W/mK
Heat Capacity	200 °C	860 J/kgK
	400 °C	960 J/kgK
	600 °C	1030 J/kgK
	800 °C	1070 J/kgK

**Tab. 2-5: Fiberfrax Durablanket S160 insulation properties**

<b>Fiberfrax Durablanket S160</b>		
Density	160 kg/m <sup>3</sup>	
Thermal Conductivity	600 °C	0.11 W/mK
	800 °C	0.16 W/mK
	1000 °C	0.21 W/mK
Heat Capacity	1000 °C	1140 J/kgK

**Tab. 2-6: ProRox WM 950 ALU insulation properties**

<b>ProRox WM 950 ALU</b>		
Density	80 kg/m <sup>3</sup>	
Thermal Conductivity	50 °C	0.039 W/mK
	200 °C	0.062 W/mK
	400 °C	0.112 W/mK
	640 °C	0.213 W/mK
Heat Capacity	50 °C	840 J/kgK

## 2.3 Reactor Vessel

The reactor vessel flow route is indicated in Figure 2-5. Cold helium enters the reactor vessel through the outer leg of the I.C (1) and flows down through the downcomer (2). The stream turn 90° in the bottom part of the RV and helium flows upstream through the heating section (3). Above the heating core, there is a hydraulic resistor made of steel plate with 7 holes with Ø18 mm. The purpose of the hydraulic resistor is to increase the pressure loss of the core. Hot helium then flows out of the RV through the inner leg of the primary coaxial pipe (5).

The heating core is composed of 7 heating assemblies (HA). Each HA has 18 ceramic channels with a helical resistive tube made of Kanthal AF. Thus, there are 126 heating channels. The diameter of the heating wire is 3.75 mm, the helical pitch is 7.5 mm, vertical length is 1 m. The ceramic channels have dimensions Ø26×3 mm, the material is mullite-alumina ceramics with 80 % of Al<sub>2</sub>O<sub>3</sub>.

Route	Description
1	Cold Helium inlet. OD = 193.7 mm, ID = 168.3 mm.
2	Cold Helium annular downcomer. OD 560 mm, ID = 513 mm.
3	Heated core (126 heating channels made of ceramic tube $\varnothing 26 \times 3$ with Kanthal wire).
4	Hydraulic resistor made of plate with 7 holes $\varnothing 18$ mm
5	Hot helium outlet, D = 90.1 mm

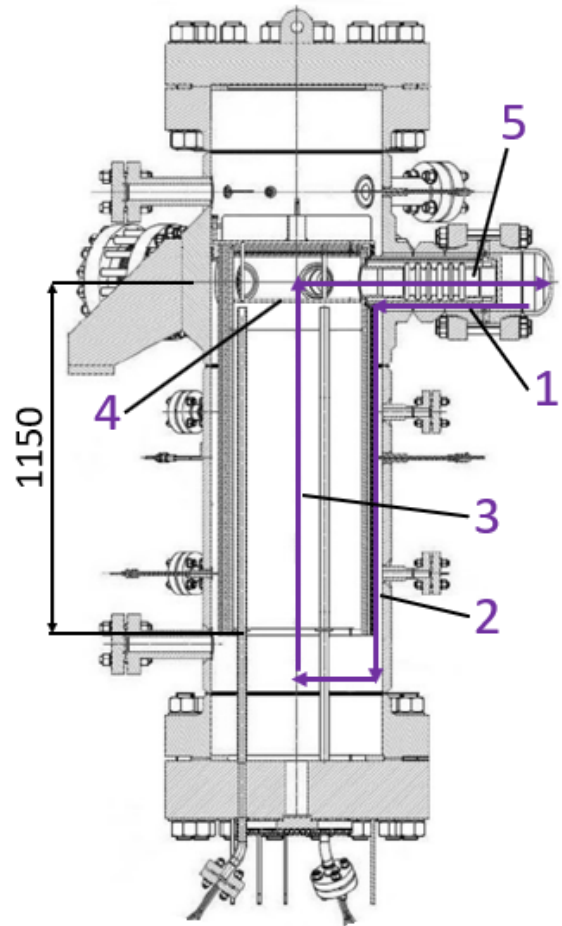


Figure 2-5: Reactor vessel flow route

Geometric parameters of the RV structures are shown in Figure 2-6. Insulation between the downcomer and the core (ID = 422 mm, OD = 513 mm) is composed of static helium and steel tubes. The RV has dimension  $\varnothing 620 \times 30$  mm. There are two layers of thermal insulation ( $2 \times 100$  mm thick) on the outer surface of the RV. The inner layer is made of Fiberfrax Durablanket S160, the outer is ProRox WM 950 ALU.

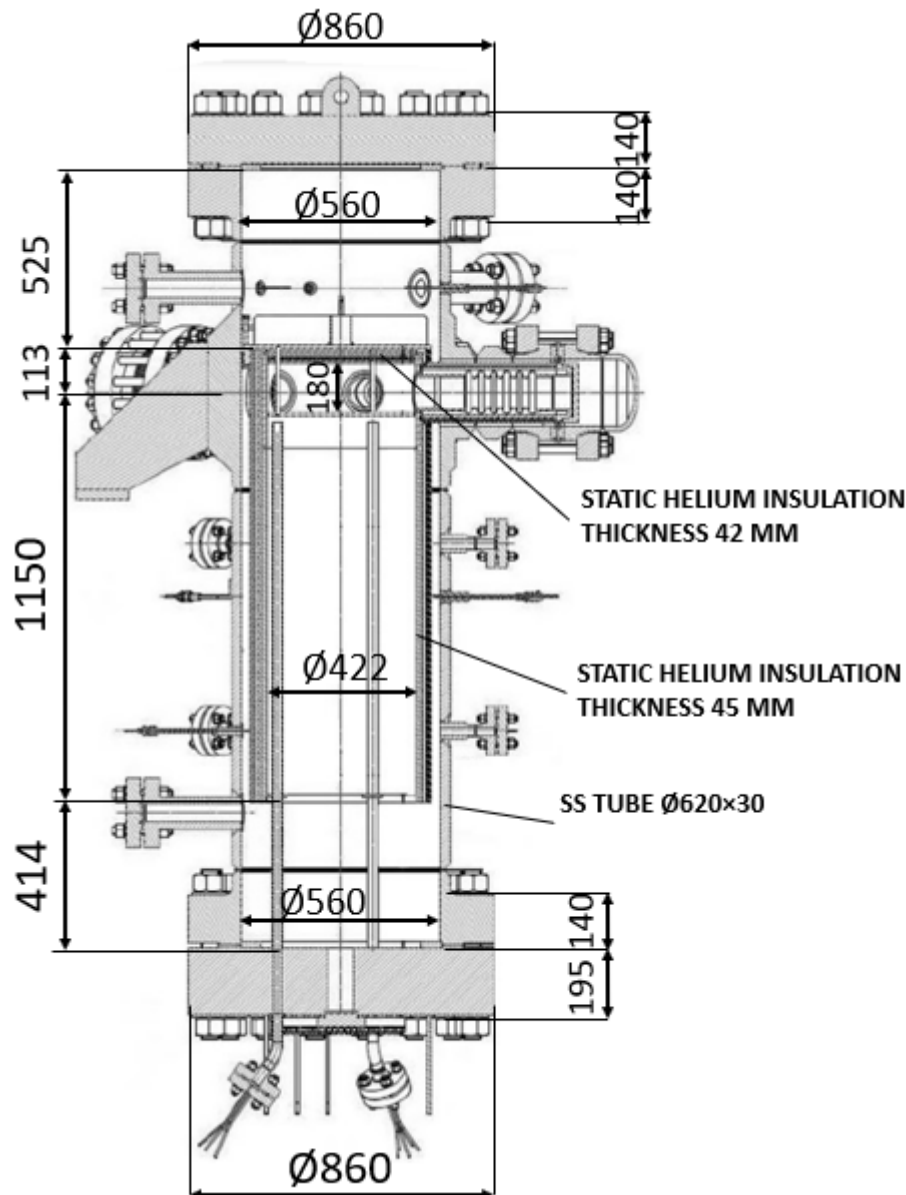


Figure 2-6: Geometric parameters of the reactor vessel

## 2.4 Primary Heat Exchanger

The PHX is the most complex and the biggest component from the geometric point of view. The diameter is approx. 1.5 m and height is approx. 5 m. The large dimensions of the heat transfer area are given by relatively high convective heat transfer resistance at both sides (gas-gas HX). The primary helium flows in the tube side, secondary helium in the shell side. The flow route is indicated in Figure 2-7.

The primary (hot) helium enters from the bottom through the inner leg of the coaxial pipe (1 purple in Figure 2-7) and flows through the tube sheet on the tube side (2 purple). The tube side is made of 268 helical tubes. The coil length is 2.3 m, each tube has 4.895 m. In the top part, the tubes turn  $180^\circ$  and are guided downwards through the outer annular volume (3 purple). The heat transfer and pressure loss in this part is low as the tubes are straight and low velocity flow is reached in the shell side. Helium exits the component through the outer leg of the coaxial pipe (4 purple). The secondary (cold) helium enters the shell side through the outer leg of the

secondary pipe (1 orange). It flows downwards through the outer downcomer (2 orange) and then turns 180° and flows upwards through the upcomer (3 orange, thermally coupled with 3 purple). The flow path 4 orange corresponds to the main heat transfer volume (thermally coupled with 2 purple). Secondary helium leaves the PHX through the central upcomer (5) into the inner leg of the secondary pipe.

Route	Description
1	Primary side (hot side) inlet. D = 91.6 mm.
2	Tube side, the main heat exchanging part. 268 helical tubes, OD 10.2, ID 5.6. Coil ID 178.5, coil OD 342.3. Radial pitch 11.5 mm, axial pitch 13 mm (angle 28 °). Coil height 2.3 m, tube length 4.895 m.
3	Tube side downcomer. 268 straight tubes OD 10.2, ID 5.6. Length 2.9 m. Low heat exchange between the primary and secondary side.
4	Primary side outlet. Annulus ID = 168.3 mm, OD 193.7, length 0.5 m.
1	Secondary side (cold side) inlet. Annulus ID = 168.3 mm, OD 193.7, length 0.37 m.
2	Secondary side external downcomer. Annulus ID = 810 mm, OD 850, length 2.6 m. No heat exchange between primary and secondary fluid, only heat losses.
3	Secondary side upcomer. Annular shell side thermally coupled with primary route 3 (low heat Exchange). Additional heat exchange between secondary side route 2 and 3. ID = 530 mm, OD 800, length 3 m.
4	Secondary side shell side thermally coupled with primary route 2. Annular shell side ID = 168 mm, OD 355, length 2.3 m.
5	Secondary side inner upcomer (outlet). D = 91.6 mm. Length 4.2 m. Additional heat exchange between secondary side route 4 and 5.

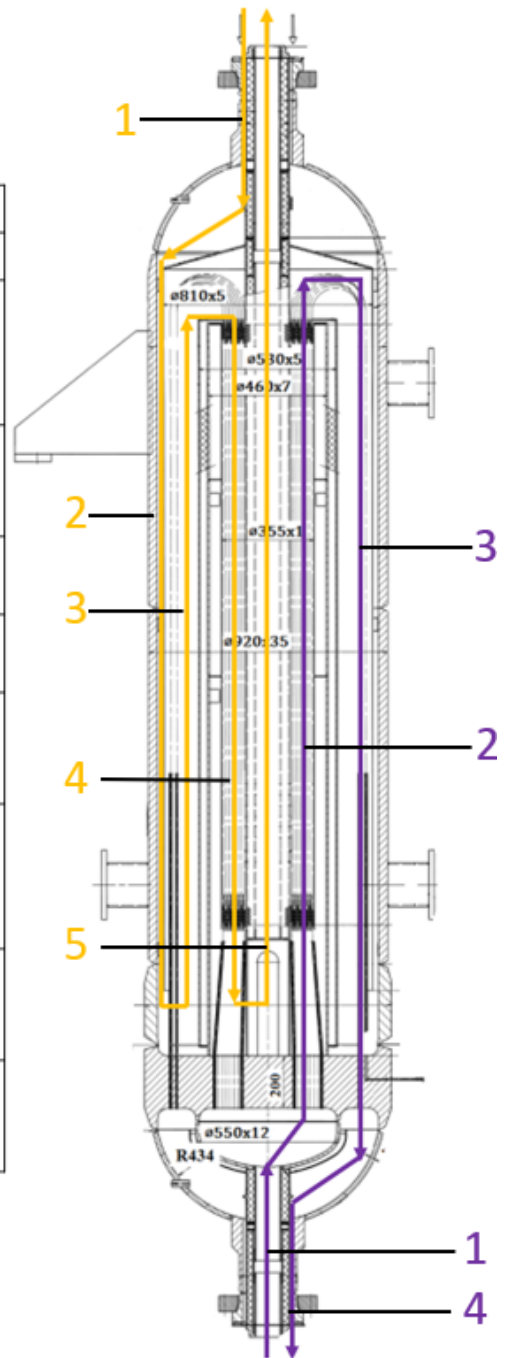


Figure 2-7: Flow route in the primary HX

The solid bodies in the PHX are described in Figure 2-8. There is an insulation layer between the inlet/outlet tubes (1). The external pressure tube has dimensions of 920×35 mm (2), two-layer insulation (2× 100 mm) is applied on the outer surface (7). There is also insulation composed of solid insulation and static helium between the downcomer and the main heat transfer volume (4,5). The primary side components (tubes) are made of Alloy 800 HT, the shell side parts are made of stainless steel 321.

Body	Description
1	Insulation ID = 101.6 mm, OD = 168.3 mm (Promalight 1000X)
2	External tube ID 850 mm, OD 920 mm
3	Tube ID 800 mm, OD 810 mm
4	Insulation ID = 470 mm, OD = 530 mm (Promalight 1000X)
5	Static helium ID = 355 mm OD = 444 mm
6	Tubesheets 200 mm thickness
7	Two-layers external insulation (2 × 100 mm). Inner layer Fiberfrax Durablanket S160, outer ProRox WM 950 ALU.

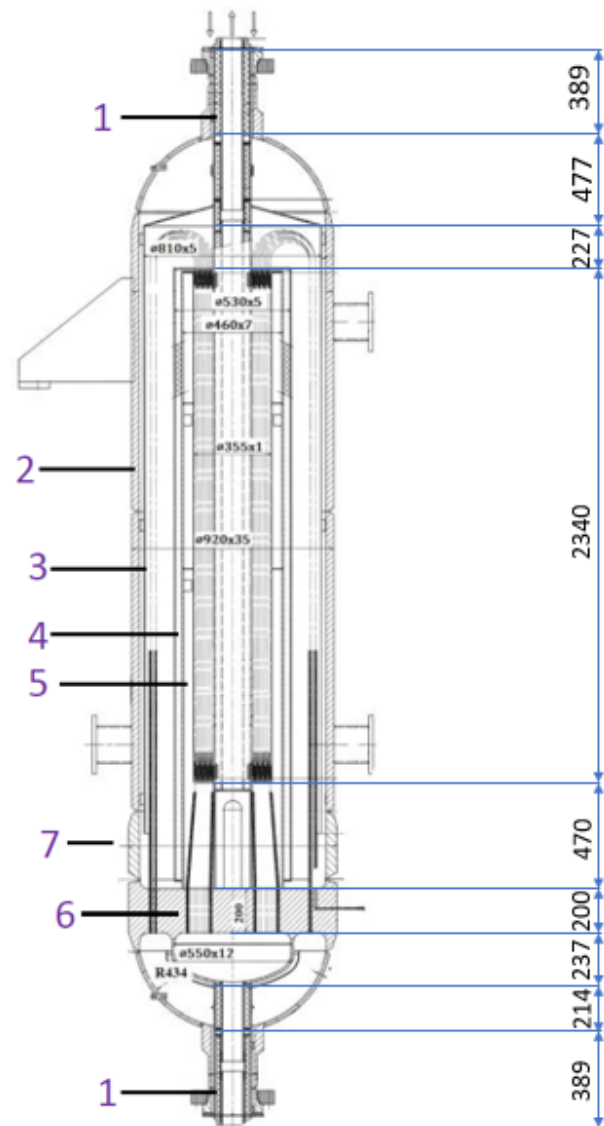


Figure 2-8: Solid bodies of the primary HX

## 2.5 Secondary Heat Exchanger

The secondary HX transfers heat from the secondary helium (tube side) to the tertiary water circuit (shell side). Although both the primary and secondary HX are designed to the nominal power of 1.05 MW, dimensions of the secondary HX are smaller due to intensive heat transfer properties at the water side.

The flow route is described in Figure 2-9. The secondary helium (tube side) enters through the inner leg (1 purple), goes into the U-tubes (2 purple) and leaves the SHX through the bottom part into the outer leg of the secondary pipe (3 purple). The tertiary water flows from the bottom to the top. The cross flow is ensured by 6 baffles. The secondary tubes are made of Alloy 800 HT, the shell components are made of stainless steel 321.

Route	Description
1	Secondary helium side (hot side) inlet. D = 91.6 mm.
2	Tube side, secondary helium, the main heat exchanging part. 57 × U-tube, OD 16 mm, ID 11 mm, average tube length 1.588 m, average tubes pitch 21 mm.
3	Secondary helium side (hot side) outlet. Annulus ID = 168.3 mm, OD 193.7.
1	Tertiary water side (cold side) inlet. ID 107.1 mm, length 0.2 m.
2	Tertiary water side – shell side, the main heat exchanging part. ID 285 mm. 6 baffles to ensure cross flow. Baffles vertical pitch 100 mm.
3	Tertiary water side (cold side) inlet. ID 107.1 mm, length 0.15 m.

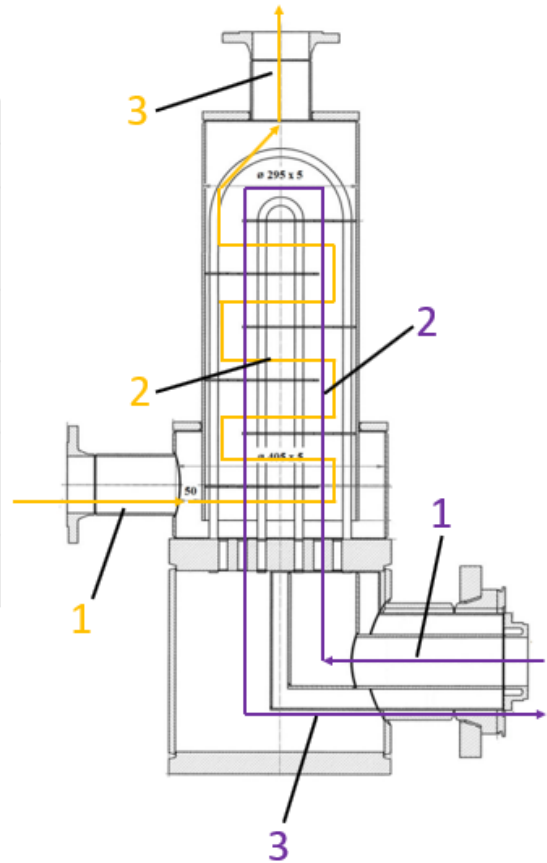
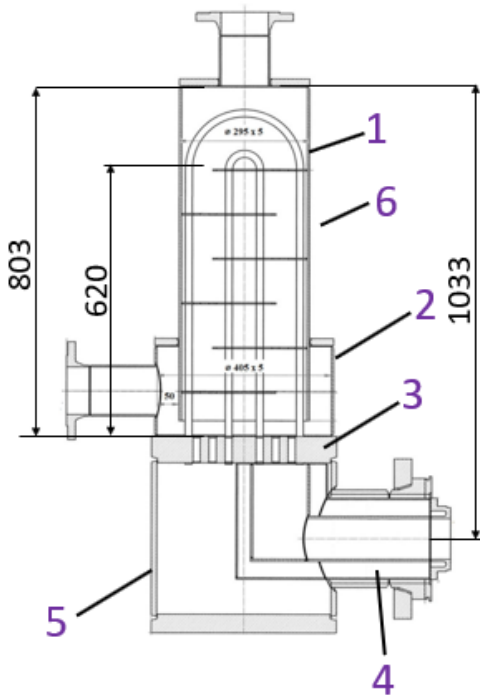


**Figure 2-9: Flow route in the secondary HX**

The solid bodies are described in Figure 2-10. The thermal insulation is applied similarly to the PHX.



Body	Description
1	Water side external tube ID = 285 mm, OD = 295 mm (stainless steel 321)
2	Water inlet manifold external tube ID = 395 mm, OD = 405 mm (stainless steel 321)
3	Tube sheet thickness 60 mm, stainless steel
4	Insulation between helium coaxial ducts ID = 91.6 mm, OD = 168.3 mm (Promalight 1000X)
5	Helium outlet manifold ID = 400, OD = 432 (stainless steel)
6	Two-layers external insulation (2 × 100 mm). Inner layer Fiberfrax Durablanket S160, outer ProRox WM 950 ALU.

**Figure 2-10: Solid bodies in the secondary HX**

## 2.6 DHR Heat Exchanger

The DHR HX is located at the top part of the DHR circuit and is intended for removing the heat from the RV during the DHR loop operation. The primary helium flows at the tube side, the shell side medium is water from the tertiary circuit. The design power of the DHR HX is 47 kW.

The flow route is relatively simple. Hot helium enters upwards through the central part of the DHR HX (1 purple in Figure 2-11), then turns 180° and flow downwards through the annular downcomer (2 purple), which is the main heat exchanging part. The cooling water flow from bottom to top through the external annular upcomer (1 green) and removes heat from the helium. The solid bodies are also described in Figure 2-11. The external tube is made of stainless steel 321, the inner parts are made of austenitic steel 310 S.

Route	Description
1	Helium side (hot side) inlet. D = 90.2 mm.
2	Helium side annular downcomer (main heat exchanging part). OD 193.7, ID = 182 mm.
1	Water side (cold side), annular upcomer. OD 242, ID = 219.1 mm.

Solid Bodies Description
Insulation between helium route 1 and 2 – composed of the steel tubes ( $\varnothing 101.6 \times 5$ and $\varnothing 182 \times 3$ ) and Promalight 1000X solid insulation between them.
Steel tube between helium downcomer and water side ( $\varnothing 219.1 \times 12.7$ )
External tube ( $\varnothing 250 \times 4$ )
Thermal insulation on the external tube. Two-layers external insulation (2 × 100 mm). Inner layer Fiberfrax Durablanket S160, outer ProRox WM 950 ALU.

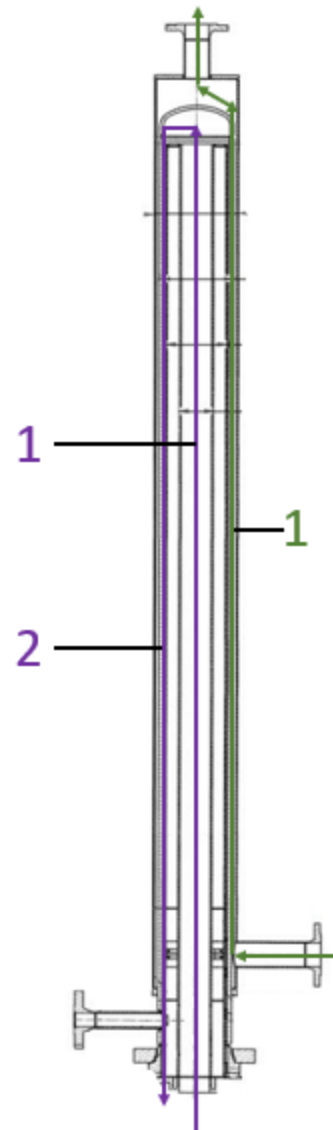


Figure 2-11: Flow route and solid bodies in the DRH HX

## 2.7 Compressors

Unique helium blowers were developed exclusively for the S-Allegro facility. The primary and secondary blowers are of the same design and are designed as one-stage radial high-speed

turbocompressors ensuring flow rate up to 0.5 kg/s and nominal compression of 1 bar. Another blower is connected to the DHR circuit and to ensure combined convection in the DHR circuit. This blower is also designed as a radial compressor but is much smaller and provides a maximum flow rate of 0.044 kg/s.

The compressors should be modelled through the operational characteristics. The nominal characteristics provided by the supplier for the primary and secondary compressors are shown in Tab. 2-7. PR is the pressure ratio and P is the inner power that can be used for helium heating due to the compressor's work.

**Tab. 2-7: Nominal characteristics of primary and secondary circulators and corresponding non-dimensional numbers**

Rotor diameter		63 mm			
Inlet pressure		7 MPa			
Inlet temperature		460 °C			
Speed		70 000		Non-dimensional numbers	
<b>m [kg/s]</b>	<b>PR</b>	<b>P [W]</b>	<b>Φ</b>	<b>χ</b>	<b>Σ</b>
<b>0.2188</b>	<b>1.019</b>	<b>5657</b>	0.026	0.552	0.485
<b>0.2625</b>	<b>1.019</b>	<b>6762</b>	0.032	0.550	0.483
<b>0.3500</b>	<b>1.018</b>	<b>8657</b>	0.042	0.528	0.464
<b>0.4375</b>	<b>1.017</b>	<b>10059</b>	0.053	0.491	0.431
<b>0.5250</b>	<b>1.015</b>	<b>10669</b>	0.063	0.434	0.381
<b>0.6125</b>	<b>1.013</b>	<b>10433</b>	0.074	0.364	0.319
<b>0.7000</b>	<b>1.010</b>	<b>9041</b>	0.084	0.276	0.242
<b>0.7875</b>	<b>1.006</b>	<b>6435</b>	0.095	0.174	0.153
<b>0.8750</b>	<b>1.002</b>	<b>2293</b>	0.105	0.056	0.049

For different operational regimes, the characteristics can be recalculated using non-dimensional numbers according to the following equations, where  $\dot{V}^*$ ,  $p^*$  and  $P^*$  are non-dimensional volumetric flow rate, pressure and power. The non-dimensional number calculated from the nominal characteristics are listed in Tab. 2-7.

$$\dot{V}^* = \Phi = \frac{\dot{V}}{2\pi ND^3}$$

$$p^* = \chi = \frac{dh_{ie}}{u^2}$$

$$P^* = \Sigma = \frac{dh}{u^2}$$

$$SVR = \frac{\rho_d}{\rho_i}, \frac{SVR_t}{SVR_{sp}} \in (0.95; 1.05)$$

The nominal characteristics and non-dimensional numbers for the DHR circulator are summarized in Tab. 2-8.

**Tab. 2-8: Nominal characteristics of DHR circulator and corresponding non-dimensional numbers**

Rotor diameter		40 mm			
Inlet pressure		7 MPa			
Inlet temperature		190 °C			
Speed		140 000 rpm		Non-dimensional numbers	
<b>m [kg/s]</b>	<b>PR</b>	<b>P [W]</b>	<b>Φ</b>	<b>χ</b>	<b>Σ</b>
<b>0.0236</b>	<b>1.00842</b>	<b>278</b>	0.0035	0.0959	0.1370
<b>0.0263</b>	<b>1.00838</b>	<b>308</b>	0.0039	0.0955	0.1364

<b>0.0350</b>	<b>1.00804</b>	<b>393</b>	0.0052	0.0915	0.1308
<b>0.0398</b>	<b>1.00766</b>	<b>426</b>	0.0059	0.0872	0.1246
<b>0.0438</b>	<b>1.00724</b>	<b>443</b>	0.0065	0.0824	0.1177
<b>0.0525</b>	<b>1.00605</b>	<b>444</b>	0.0078	0.0689	0.0984
<b>0.613</b>	<b>1.00451</b>	<b>387</b>	0.0092	0.0514	0.0734
<b>0.7000</b>	<b>1.00253</b>	<b>248</b>	0.0105	0.0288	0.0412

Validity of the non-dimensional number should be checked for each specific case. Allowable machine Mach number departures and specific volume ratios should fit within the limits. The check will be done by the benchmark organizer for each experimental case so only the experiments with valid operational conditions will be presented.

## 2.8 Coaxial valves

There are two special coaxial valves. So called cross-valve is installed in the bottom part of the DHR loop (Figure 2-12). The cross-valve allows straight flow in both legs of the coaxial pipe in an “open” state (corresponding to the DHR operation) while in the “crossing” state, it ensures a small portion of helium to flow from the reactor vessel inside the inner leg of the DHR loop. The purpose of the crossing state is preconditioning of the DHR loop. The second disk valve is installed in the primary loop between the reactor vessel and the primary circulator (Figure 2-12). The function of this component is to allow normal flow through the primary circuit during the nominal primary loop operation and to close the primary loop during the DHR loop operation.

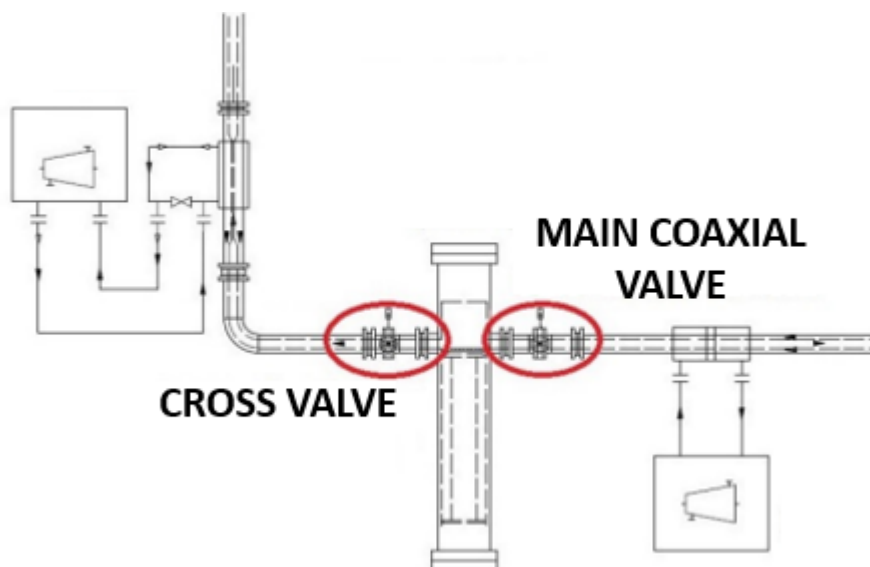


Figure 2-12: Location of the coaxial valves

For the preparation of the numerical model using a systemic code, it is not necessary to model these components in detail. The pressure loss in an open state should be relatively low, the impact on temperature development is only given by its thermal inertia (mass approx. 240 kg of stainless steel). It is however important to understand their function. The main coaxial valve in both positions is shown in Figure 2-12.

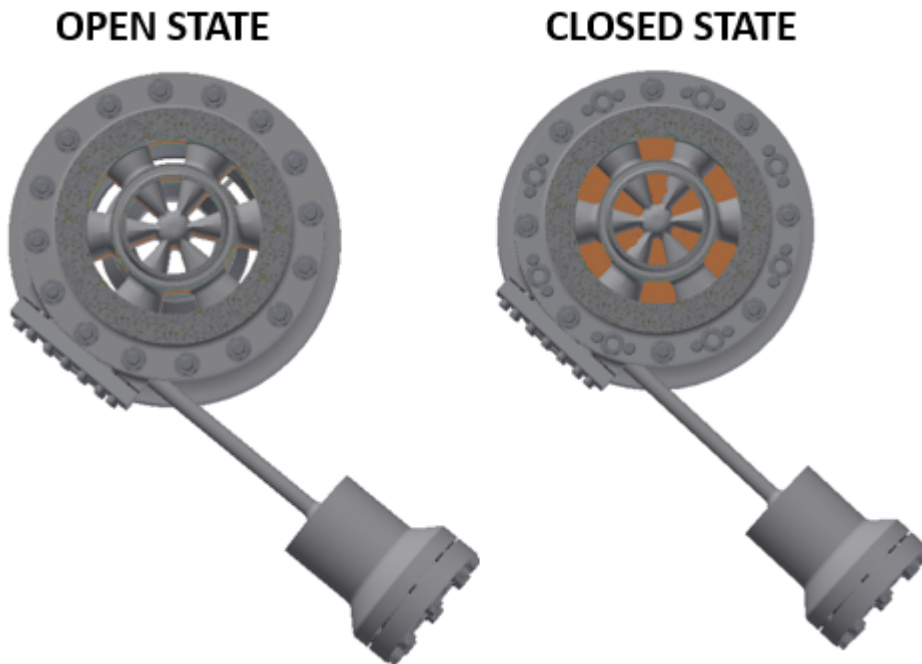


Figure 2-13: Main coaxial valve

## 2.9 Tertiary circuit

---

The tertiary circuit uses cooling water from the existing cooling system that is used also for other technologies in the experimental hall. The same circuit is used for the removal of the heat from both the SHX and DHR HX. It is recommended to model only the shell side of both HXs and use experimental data as the inlet boundary conditions, not to model the whole tertiary circuit. This approach should be sufficient as the III.C is usually controlled to the constant flow rate and inlet water temperature. The water flow rate is usually high enough so the temperature gain is very low.

## 2.10 Other systems

---

There are several auxiliary systems that should be mentioned but might not be considered in the models for the purposes of this particular benchmark. Relatively simple experiments with no impact of such systems will be considered in this activity. They might be however involved in potential future modelling tasks with a higher level of detail.

Filling and draining of both the helium circuits is performed using a helium storage system consisting of pressure bottles. Before an experimental campaign, both circuits are filled to an appropriate cold-state pressure level. The target pressure is then reached by heating of the system. During the draining, the helium outgoing from the loop is cooled in the auxiliary HXs and is stored in the storage system. There are also several auxiliary HXs used for cooling of the helium during draining.

The important function of the S-Allegro is a simulation of the accidental scenarios. Two dedicated systems were implemented for the simulation of the accidental scenarios. Four LOCA valves are located in the I.C allowing controlled leakage from the loop to simulate LOCA conditions with a prescribed pressure gradient. A system intended for the simulation of a severe accident mitigation system based on the injection of heavy gas in the DHR circuit is also

implemented. Injection of heavy gas in the system may help to establish the natural convection in the system by increasing the density difference between the cold and hot leg of the DHR loop. Other accidental scenarios might be simulated using the inherent features of the component. For example, a LOFA accident might be simulated by a controlled decrease of the main circulator power, failures of the valves may be simulated by controlled closing/opening of such a component.

## 2.11 Instrumentation

---

Various types of instrumentation for both experimental and control purposes are implemented. Temperature sensors are intended for the measurement of the temperature field in the loops. The temperature measurement is refined especially in the RV and the DHR circuit. Other thermocouples are placed on the surface of the pressure equipment to ensure safe operation. More than 60 temperature sensors are distributed all over the facility. In each circuit, pressure level and mass-flow rate are measured. Additional pressure difference sensors are used for the measurement of local pressure drops (e.g. at circulators). The heating power of the RV is measured by a power meter. Other auxiliary sensors are utilized for control of the individual components (speed meters for control of the circulator, position sensors for control of the valves). The facility is operated from a control room located in the experimental hall. The measured data are stored in a DAQ system with selectable time steps.

For this benchmark purpose, several sensors were selected that are relevant for the comparison with the experiments. The layout of the instrumentation is shown in Figure 2-15, the layout of the temperature sensors at the outlet of the heating core is in Figure 2-14.

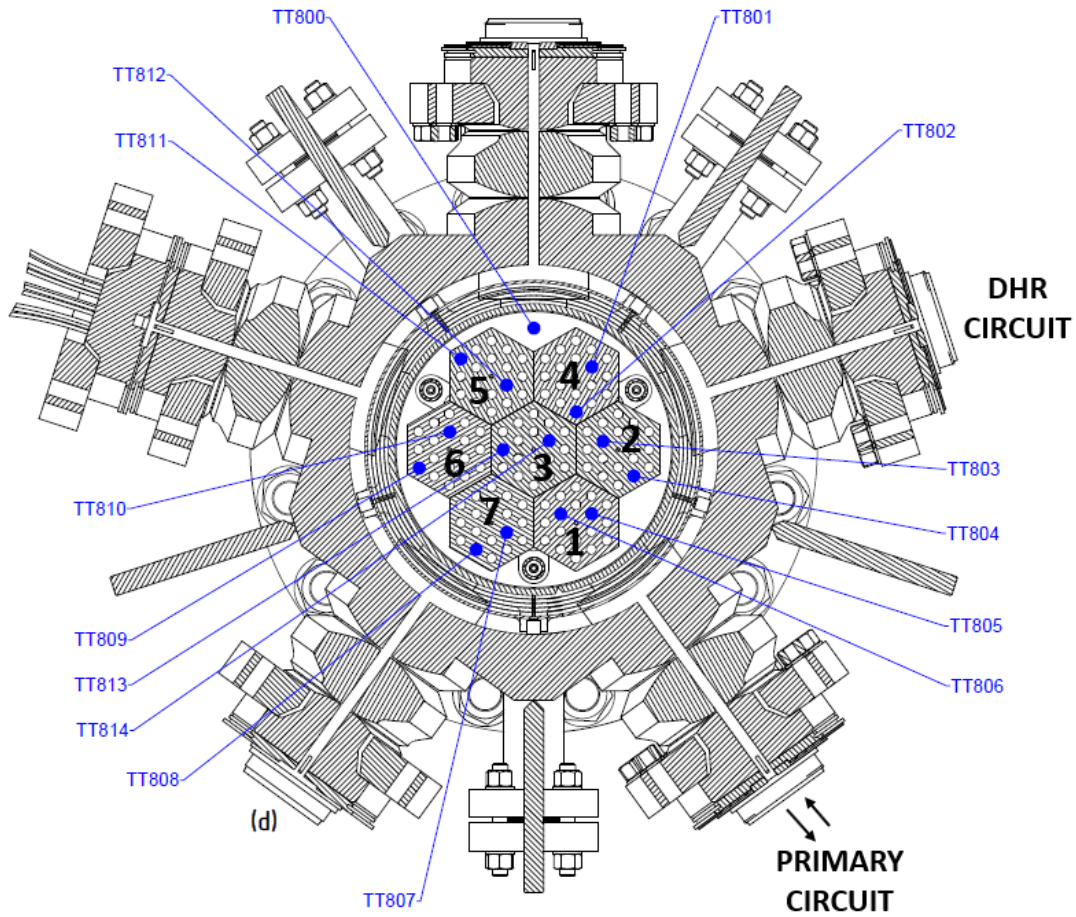


Figure 2-14: Temperature sensors at the outlet of the heating core

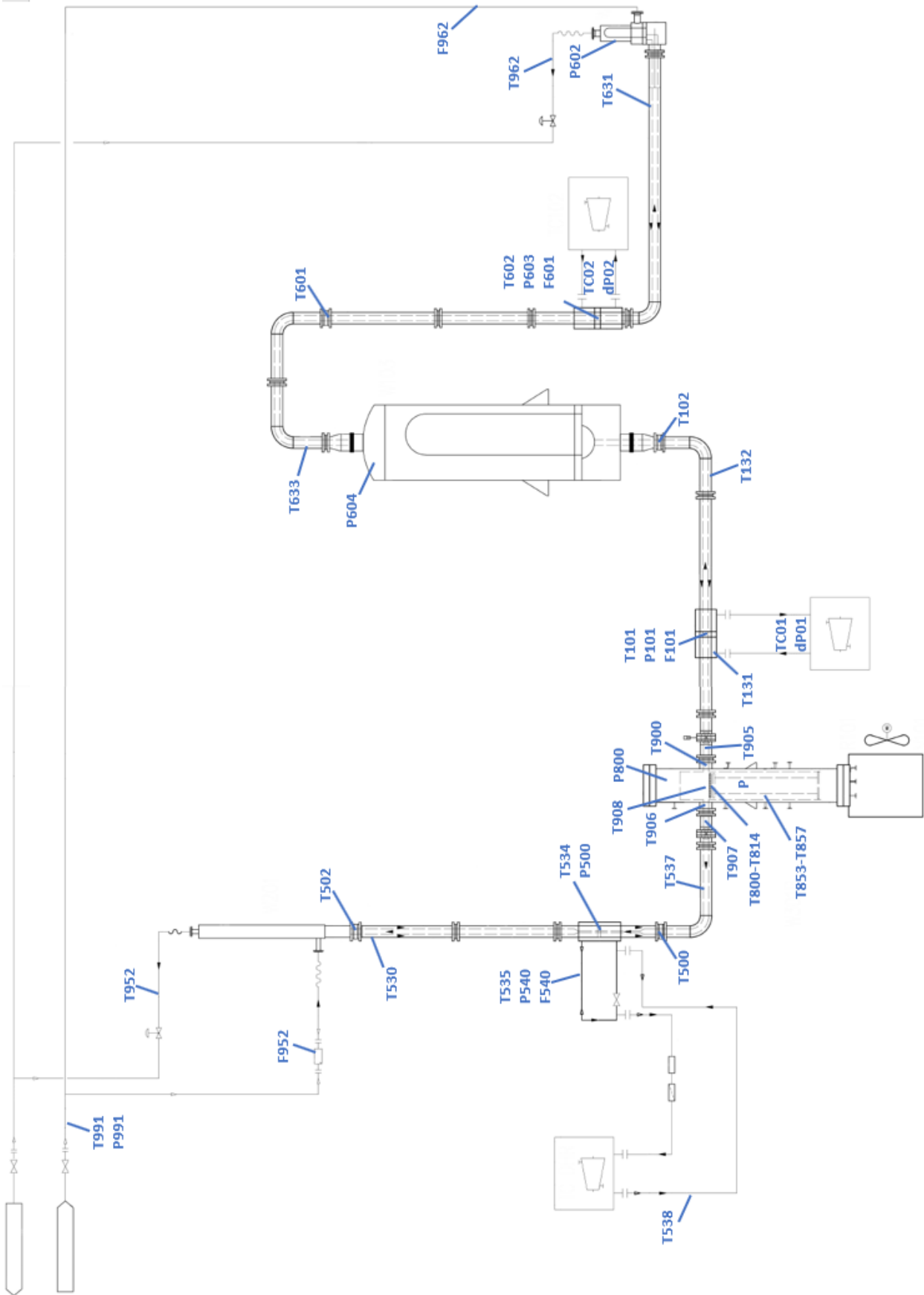


Figure 2-15: Instrumentation layout

A description of the sensors according to Figure 2-15 including sensor types is in Figure 2-15. All temperature sensors for helium are K-type thermocouples.

**Tab. 2-9: List of instrumentation for benchmark**

<b>Sensor</b>	<b>Description</b>
T101	He temperature – inner leg I.C
P101	He pressure – inner leg I.C (Cerabar S PMP71)
F101	He mass-flow rate – inner leg I.C (differential pressure Torbar)
T132	He temperature – outer leg I.C – PHX outlet
T102	He temperature – inner leg I.C – PHX inlet
TC01	Primary circulator speed
dP01	Primary circulator PR (Deltabar S PMD 75)
T900	He temperature – inner leg I.C – RV outlet
T905	He temperature – inner leg I.C – RV outlet
T853-857	He temperature – RV downcomer (circumferentially)
T800-814	He temperature – outlet of the heating sections
T908	He temperature – above the hydraulic resistor
P800	He pressure in the RV - outer leg (Cerabar S PMP71)
P	Heating power
P604	He pressure in the PHX – I.C (Cerabar S PMP71)
T633	He temperature – outer leg I.C – PHX inlet
T601	He temperature – inner leg I.C – PHX outlet (differential pressure Torbar)
T602	He temperature – inner leg I.C
P603	He pressure – inner leg I.C (Cerabar S PMP71)
F601	He mass-flow rate – inner leg I.C (differential pressure Torbar)
TC02	Secondary circulator speed
dP02	Secondary circulator PR (Deltabar S PMD 75)
T631	He temperature – outer leg I.C – SHX outlet
P602	He pressure – SHX (Cerabar S PMP71)
T962	Water temperature – SHX outlet
F962	Water flow rate in SHX (Promag 10L80)
T906	He temperature – inner leg DHR – RV outlet
T907	He temperature – inner leg DHR – RV outlet
T537	He temperature – outer leg DHR
T500	He temperature – inner leg DHR
T534	He temperature – inner leg DHR
P500	He pressure – inner leg DHR (Cerabar S PMP71)
T535	He temperature – outer leg DHR – DHR circulator
P540	He pressure – outer leg DHR – DHR circulator (Cerabar S PMP71)
F540	He mass-flow rate – outer leg DHR – DHR circulator (differential pressure Deltatop)
T538	He temperature – outer leg DHR – DHR circulator outlet
T530	He temperature – outer leg DHR – DHR HX outlet
T502	He temperature – inner leg DHR – DHR HX inlet
T952	Water temperature – inner leg DHR – DHR HX outlet (Pt100)
F952	Water flow rate in DHR HX (Promag 10L80)
T991	Water inlet temperature (Pt100)
P991	Water inlet pressure (Cerabar PMP11)

### 3 DESCRIPTION OF EXPERIMENTS AND DATA FOR BENCHMARKING

In this section, the data for the codes benchmarking will be described. This section will be updated with new experimental data once collected.

#### 3.1 Nominal parameters

In the first phase, the computational models can be compared with the “nominal” (maximum) parameters of the S-Allegro. These parameters are summarized in Tab. 3-1. The values are based on the design parameters, not on experimental data.

**Tab. 3-1: Nominal design parameters**

T132	445 °C
T131	450 °C
T900	850 °C
F101	0.5 kg/s
P101	7 MPa
T633	360 °C
T631	365 °C
T601	820 °C
F601	0.445 kg/s
P604	6.5 MPa
P	1 050 kW
P991	0.5 MPa
T991	30 °C
T962	45 °C
F952	17 kg/s

#### 3.2 Steady-state data on heat exchangers

The data were collected during the previous operation of the S-Allegro. Four steady-states that might be used for check of the HXs models were collected. As the PHX and SHX are the most complex components, it is recommended to test the HX models on the available data.

**Tab. 3-2: Data for heat exchangers benchmarking**

T101	145.4	133.1	169.9	280.3
T102	141.8	129.6	164.9	273.3
P101	3.11	3.04	3.25	3.58
F101	0.223	0.247	0.222	0.245
T132	79.0	57.2	63.9	141.1
F601	0.197	0.497	0.499	0.192
P604	3.14	3.0	3.05	3.71
T601	44.1	48.6	53.4	69.5
T633	117.9	84.2	99.8	230.9
T602	117.1	82.3	101.4	223.2
T631	40.4	45.2	50.1	60.4
F962	2.79	2.76	2.8	3.61

P991	0.58	0.57	0.57	0.56
T962	27.0	31.3	32.5	32.3
T991	20.4	22.7	21.8	21.6

### **3.3 Steady-state data – primary loops operation**

---

The data will be added after the S-Allegro operation in 2023.

### **3.4 Transient data**

---

The data will be added after the S-Allegro operation in 2023.

## 4 CONCLUSION

In this document, S-Allegro facility is described in order to allow its modelling using systemic codes by the benchmark participants. Needed geometrical, material and operational parameters are given. Also the experimental data that might be used for the first check of the computational models and individual components are presented. As the main operational campaign in S-Allegro is scheduled for 2023, the report will be updated later once all data for the benchmark are collected. The benchmark results will be summarized in the following deliverable D5.4.

The purpose of this deliverable is to initiate the STH benchmark activity. Regular meetings of the benchmark participants will be organized to discuss progress in modelling. Based on the potential requirements of the benchmark participants or missing parameters, the report might be further updated.

Moreover, a CFD benchmark was organized by BME within this activity. A description of this benchmark including the experimental data is attached to this report.

# ATTACHMENT NR. 1 - ALLEGRO CFD BENCHMARK

BME-NTI-980/2022

## ALLEGRO CFD BENCHMARK

### PART 1

#### Flow Straightener Benchmark Description



**BUDAPEST UNIVERSITY OF TECHNOLOGY AND ECONOMICS (BME)**  
**Institute of Nuclear Technics (NTI)**

Name	Occupation	Institution	Contact
<b>Gergely Imre Orosz</b>	<b>PhD student</b>	<b>BME NTI</b>	<b>orosz@reak.bme.hu</b>
Mathias Peiretti	MSc student	BME NTI/ Politecnico di Torino	matthias.peiretti@edu.bme.hu
Boglárka Magyar	BSc student	BME NTI	bogi0614@gmail.com
Dániel Szerbák	MSc student	BME NTI	szerbakdani@gmail.com
Dániel Kacz	PhD student	BME NTI	kacz.daniel@reak.bme.hu
Béla Kiss	Research assistant	BME NTI	kiss@reak.bme.hu
Gábor Zsíros	Research assistant	BME NTI	zsiros@reak.bme.hu
Prof. Attila Aszódi	Professor	BME NTI	aszodi@reak.bme.hu

Budapest, Hungary, 2022.01.14.

## 1. SHORT DESCRIPTION

At BME (Budapesti Műszaki és Gazdaságtudományi Egyetem - Budapest University of Technology and Economics) NTI (Nukleáris Technikai Intézet - Institute of Nuclear Technics), a 7 pin ALLEGRO rod bundle test section has been built in order to investigate the hydraulic behavior of the coolant in such design and to develop CFD models that could properly simulate the flow conditions in the ALLEGRO core. PIRouETTE (PIV Rod bUndLE Test faciLity at bME) is a test facility, which was designed to investigate the emerging flow conditions in various nuclear fuel assembly rod bundles. The measurement method is based on Particle Image Velocimetry (PIV) with Matching of Index of Refractory (MIR) method. Despite the working fluid in ALLEGRO will be helium, in this case water is in the same Reynolds number range of the ALLEGRO rod bundle. In the test loop, it was necessary to install a flow straightener that was able to condition the velocity field before the rod bundle. The results of CFD simulations could be used to improve the understanding of the inlet conditions in the rod bundle test section.

The herein proposed benchmark deals with the 3D CFD modeling of the velocity field within the flow straightener used in this test section. The geometry of the flow straightener will be given to the participants in an easy-to-use 3D format (.tin, .stp or .stl for example).

In **Chyba! Nenašiel sa žiaden zdroj odkazov.**, an overview of the test loop is provided. It can be seen where the flow straightener is placed in order to eliminate the effect of the elbow on the fluid flow.

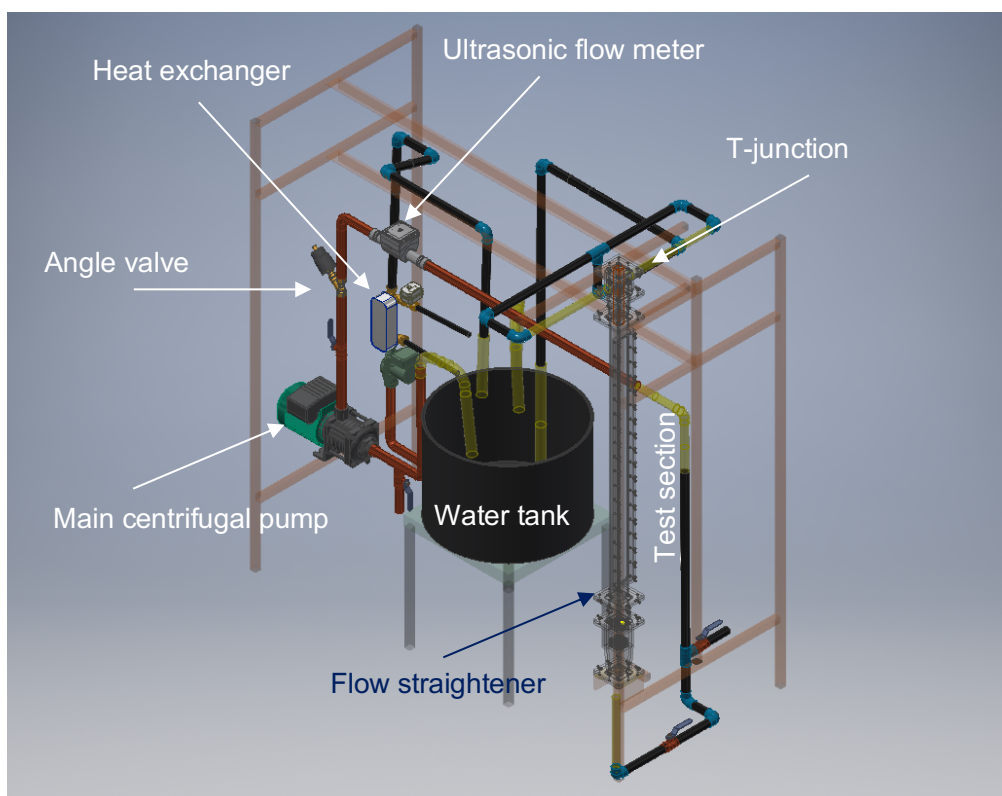


Figure 1: The structure of the PIRouETTE facility

## 1.1. TEST SECTION

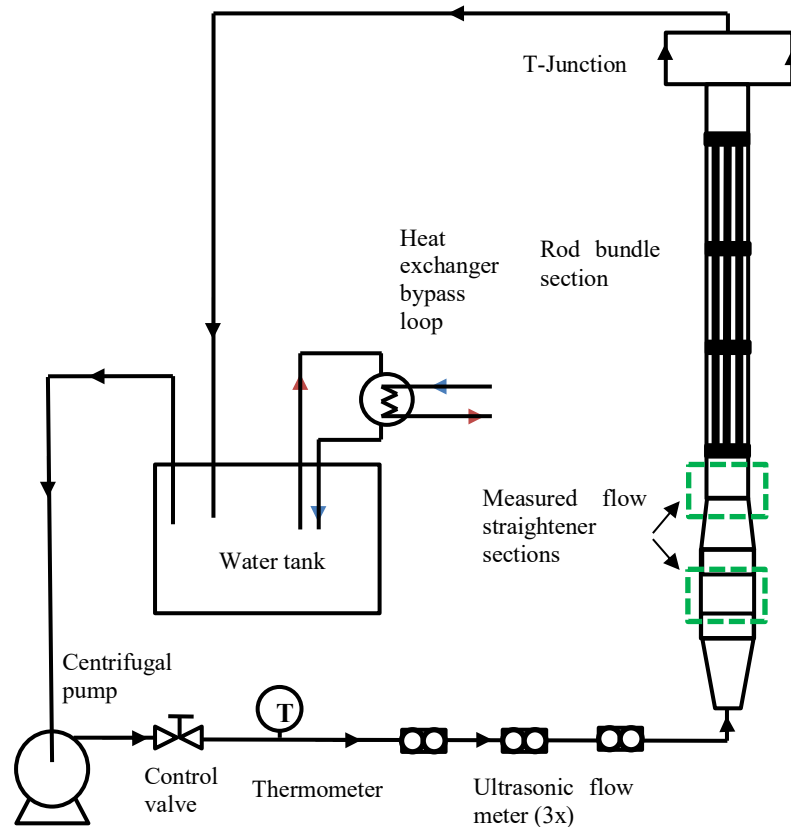


Figure 2: The schematic of the PIROUETTE facility

The structure and the main parts of the test facility can be seen in Figure 1. The installation contains a 1 meter long vertically arranged seven pin rod bundle in the test section. The water flow is provided by the main centrifugal pump (Type: Wilo MHIL 903, Power: 1.1 kW,  $Q_{\max}$ : 14 m<sup>3</sup>/h (1)). Some of the power of the centrifugal pump dissipates into the turbulent flow, causing the rise of the temperature in the test loop. To provide a constant test loop water temperature, a bypass heat exchanger loop was installed into the facility. With the heat exchanger the water temperature was controlled and kept in  $30 \pm 1$  °C during the measurements. From the pump, the medium flows to a ball valve with a nominal diameter of initially  $\frac{3}{4}$  inch (DN 32). The ball valve is not suitable for fine control of the mass flow and therefore it is followed by an angled seat valve. The fine control valve is followed by three HYDRUS ultrasonic flowmeter [2]. Multiple volumetric flow meters increase the accuracy of the volumetric flow measurement, which is very important for setting the inlet boundary condition for CFD calculations. The measuring channel section and the pump flow control subsystem are connected by a KPE pipe with an inner diameter of 26 mm. From here the water is fed through the diffuser cone to the flow straightening section. The flow straightener reduces disturbances caused by mechanical, flow control and pipe lining equipment. The 1 meter long seven-rod bundle was installed in the test channel section. A removable lid has been designed on the test section for ease of access which allows the change of the rod geometry. With this solution, different types of spacer grids and mixing vanes can be used.

A T-junction is placed after the test section; the medium discharges to the water tank through other pipes lines. The schema of the test facility can be seen in the Figure 2 and the 3D model in Figure 1.

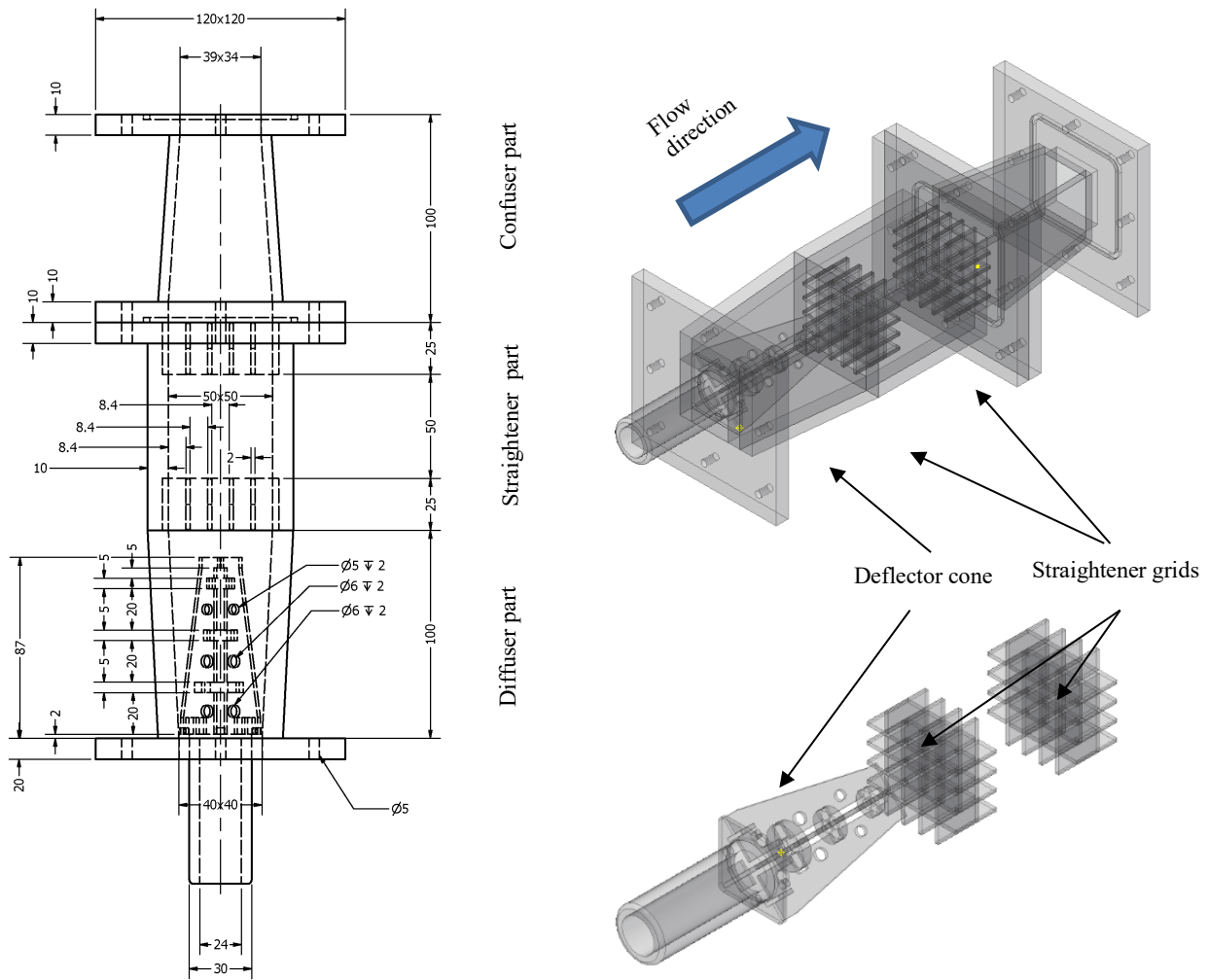


Figure 3: 3D CAD model of the flow straightener

The test section is designed to make the measurement section, the associated confuser and diffuser connectors easily interchangeable. The flow straightener includes two straightener grids and a deflector cone to restrict the flow from the effects of the pipe elbows upstream of the test-section. The cross section of the diffuser is 40x40 mm at the beginning and 50x50 mm at the end. A confuser adapter part is located above the straightener part. The cross section of the diffuser is 50x50 mm at the beginning and 39x34 mm at the end. At the exit of the confuser, the cross-section of the channel is the same as the cross-section of the measuring channel section. This avoids problems caused by sudden cross-section changes.

In the flow straightener, there is a part named deflector cone. This specific part has the purpose of disrupting the main flow jet of the inlet pipe. It contains 4 perforated trapeze-shaped plates, which are perpendicular to each other. These plates hold the 3 deflector rings, which break the flow direction and eliminate the high-speed central jet. Due to the complexity of the geometry, the exact dimensions of these parts are not provided in written form but in 3D model format.

The middle section of the flow straightener contains two straightener grids with a height of 25 mm. The distance between the grids is 50 mm. The grids are made with compartment layout. The plates are made from 2 mm thick PMMA plates with equidistant grid spacing of 8.4 mm. The cross-section of the measuring channel section exactly matches the hydraulic parameters of the reactor type under tests. Our 1 meter long bundle of rods is made of FEP (Fluorinated Ethylene Propylene) to meet the MIR criteria. The FEP polymer has a refractive index of 1.33

which is nearly the same as the refractive index of the working medium (water). The outer and inner diameter of the rod are 10/6 mm, and the inside of the rods is filled with ultrafiltrated water. The rods are connected with small metal pins into the first and fourth spacer grids, and the spacer grids are connected to the channel wall with groove fitting.

## 2. PIV SYSTEM

The PIV measurement system includes the following components:

- tracer particles: polyamide spheres with an average diameter of  $d = 50 \mu\text{m}$  (3),
- light source subsystem: Litron Nano L PIV dual Nd:YAG laser (maximum pulse energy: 135 mJ, wavelength: 532 nm, pulse length:  $\sim 6$  ns, maximum flash frequency: 15 Hz) (4),
- beam guide arm and beam forming optics (5),
- image capture subsystem (camera): SpeedSense Lab 110 high-speed digital camera, resolution: 1 megapixel (1280x800), frame rate: 1630 fps, buffer: 12 GB (6),
- Synchronizer: Dantec Timer Box (80N77) (7),
- Synchronisation, image capture and processing software: Dantec DynamicStudio, latest stabile version 6.6 (8),
- camera and beam-optics positioning systems.

## 3. MEASUREMENT PROCEDURE

The flow straightener measurements were performed in the vertical measurement section. Figure 4 shows the schematic layout of the experiment. The illuminated volume is  $\sim 1.5$  mm wide. We get information about the flow processes during the measurements from this volume. This measurement feature should also be considered during the CFD model result comparison. In the case of our current measurements, the illumination planes were positioned in the inside of the flow straightener section and other measurements were also taken at the beginning of the rod bundle test channel. The camera sees perpendicular to these planes.

Before starting the measurements, a so-called target sheet was placed in the appropriate position in the channel. The target sheet is a specially printed dotted sheet. Knowing the diameters of the dots and their positions helps to recover the real physical dimensions from the images. The coordinate axes can be identified using points of different diameters on the target. After a sufficient number of points have been detected, the conversion from pixel to millimeter distance is done automatically by a software (8). In flow straightener measurements, 2000 image pairs were recorded in the vicinity of the straightener grids. Each gap of the compartment grid was examined. We aimed to observe the flow inside the flow volume. The first 100 image pair were discarded from the 2000 images captured because the lasers have a "warm-up" time requirement; therefore, the quality of the images at the beginning of the acquisition is not good. To get a sufficiently detailed picture of the flow field, post-processing of the raw images is necessary. Figure 5 shows the steps of image processing. The first image shows the raw image (Figure 5/1). In the first step, an average image of 1900 image pairs was created (Figure 5/2). This average image was extracted from each image to reduce the effect of the elements that are present in each image (shadows, glitches and static elements) (Figure 5/3). Laser light is not uniform in intensity along the length of the illuminated plane. Figure 5/4 shows an image processed by "image balancing" to correct for this unevenness of illumination. Since not all static elements can be eliminated from the images in this way, the static parts and regions not included in the flow field have to be masked out with digital masks. The row of Figure 5/5 shows the masked image, where only the polyamide particles that move with fluid are visible. After these steps, the individual image pairs were used to create the instantaneous vector fields separately. These vector fields show the chaotic velocity distribution typical of turbulent flow (Figure 5/6). From these 1900 vector diagrams, the time-averaged vector field describing the region after the spacer was created (Figure 5/7). With this method, not only the time-averaged velocities can be obtained, but also an estimate of the temporal fluctuations of the velocity vectors. In this way, we will not only be able to assign a vector value to a given pixel, but we will also be able to know its vector statistics.

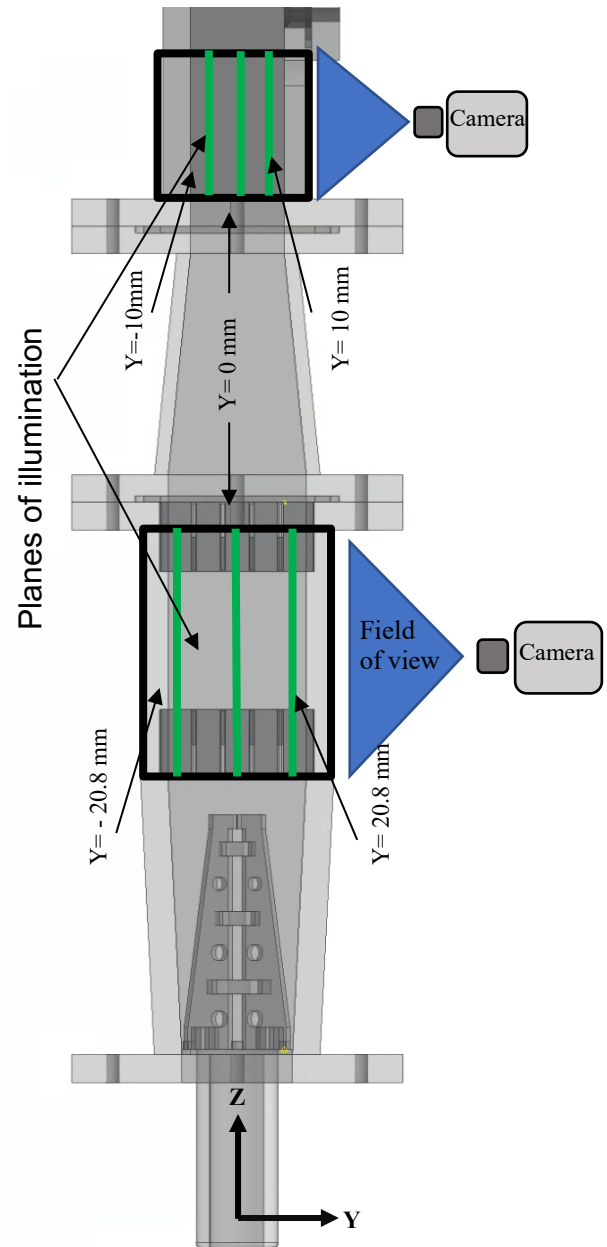


**Figure 4: Monitor planes**

The row of Figure 5/5 shows the masked image, where only the polyamide particles that move with fluid are visible. After these steps, the individual image pairs were used to create the instantaneous vector fields separately. These vector fields show the chaotic velocity distribution typical of turbulent flow (Figure 5/6). From these 1900 vector diagrams, the time-averaged vector field describing the region after the spacer was created (Figure 5/7). With this method, not only the time-averaged velocities can be obtained, but also an estimate of the temporal fluctuations of the velocity vectors. In this way, we will not only be able to assign a vector value to a given pixel, but we will also be able to know its vector statistics.

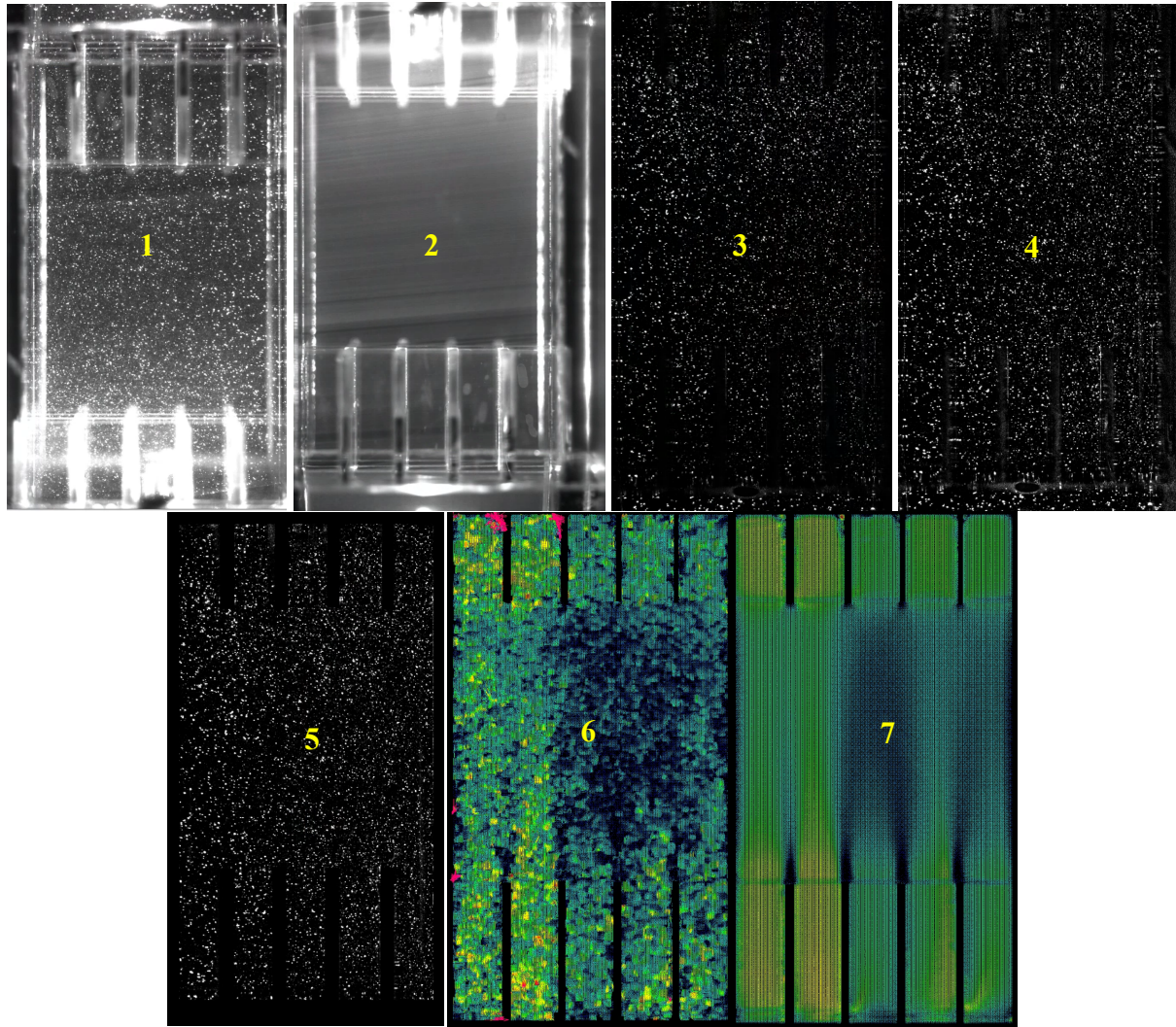


Figure 5: The steps of the image post-processing

#### 4. ESTIMATION OF UNCERTAINTY IN PIV MEASUREMENTS

In PIV measurement, the velocity of the particles flowing with the fluid is measured instead of the velocity of the flowing fluid. The density of the particles is approximately equal to the density of the liquid. The diameter of the particles in this case is 50 micrometers. Two digital images of the particle distribution are taken, from which the two-dimensional vector field can be calculated. The time interval between the two images can vary from a few microseconds to several milliseconds, depending on the velocity of the main flow.

In the interrogation areas, the velocity is assumed to be uniform during the image pair recording period. Knowing the delay between the recorded images and the displacement of the particles, the velocity vectors can be correlated to the interrogation regions using correlation methods (9).

Using calibration, the displacement (measured in pixels) can be converted to a metric value using the following formula (10):

$$u = \alpha \frac{\Delta X}{\Delta t} + \delta u \quad (1)$$

Where:  $u$  is the physical velocity [m/s],  $\alpha$  [m/pixel] is the conversion factor for magnification,  $\Delta X$  [pixel] is the displacement of the recorded image, and  $\Delta t$  [s] is the time elapsed between the two images being recorded. The magnification factor  $\alpha$  was determined by the calibration target.  $\delta u$  is difficult to detect systematically and is usually classified as an uncertainty factor rather than a measurement parameter.

In general, the measurement setup can be broken down into four subsystems:

- Calibration subsystem: converts the displacement in pixels into displacement in metric,
- Visualization: trace particles, illumination,
- Image recording: digital camera,
- Image processing: cross-correlation method, vector field calculation, etc.

The uncertainty in the target variables (flow velocities) is most affected by errors from the four subsystems.

Main parameters		Calibration	
Area investigated	105 x 50 mm <sup>2</sup>	Calibration length on target $l_{sel}$	31.5 mm
Average flow velocity $w$	2.0112 m/s	Calibration length on the visualisation plane $L_{sel}$	365 pixel
Flow cross section $A$	2500 mm <sup>2</sup>	Magnification $\alpha$	0.08630137 mm/pixel
Flow rate $Q$	1.66667 l/s		
Flow visualisation		Image recording	
Trace particle	Polyamide spheres	Kamera	
Average diameter $d_p$	0.05 mm	Resolution	1280 x 800 pixel
Average density	1.02 g/cm <sup>3</sup>	Frame rate	1690 Hz
Light source	Litron Nano L PIV duál Nd:YAG laser	Objective	Nikon 60mm f/2.8 Micro-NIKKOR AF-D
Laser power	138 mJ	Distance from the plane of illumination $l_t$	260 mm
Laser plane width	1.5 mm	Angle of perspective $\varphi$	11.41 °
Pulse frequency	15 Hz		
Time interval	50 $\mu$ s		
Data processing			
Pixel value analysis	Cross correlation method		
Interrogation area	16 x16 pixel		
Search area	8 x 8 pixel		
Sub-pixel analysis	three-point Gaussian fit		

Table 1: Some basic data for the measurement system error calculation

To achieve sufficiently accurate measurements, the estimates of random and systematic errors should be determined at the 95% confidence level and the resulting quadratic error function

should be generated. This allows us to estimate the measurement uncertainty with 95% confidence.

Each element in equation (1) is subject to systematic error and random error, which introduce bias into the result and give the uncertainty of the measured value. Using the appropriate literature, a detailed uncertainty analysis was carried out which included the following sources (11) (10) (12) (13) (14) (15):

- Error sources and sensitivity factors for magnification  $\alpha$ 
  - o Reference length identification
  - o Error caused by the image recording system
  - o Error due to de-warping was neglected
- Error sources and sensitivity factors of  $\Delta X$  image displacement
  - o Error due to illumination
  - o Error caused by the image recording system
  - o Image processing, calculation of displacement
- Error sources and sensitivity factors of  $\Delta t$  time delay
  - o Error sources of the delay generator (timer) timing
  - o Error sources of the laser pulse timing
- Error sources and sensitivity factors of  $\delta u$  velocity difference
  - o Flow following ability of the particles (trajectory)
  - o Three-dimensional effects
  - o Uncertainty due to volume flow adjustment
- The effect of sampling

At most points in the flow field, the error of our measurement is  $\sim 0.17$  m/s. This relative error is naturally larger in the lower velocity sections (along walls), since most of the sources of error in the uncertainty analysis are constant, and few depend on the actual velocity vector of the measured flow. The uncertainty values fitted to the measurement points are included in the data series sent out.

The experimental data are available in .xls format and will be distributed directly to the participants. Please write an e-mail to **Gergely Imre Orosz** <[orosz@reak.bme.hu](mailto:orosz@reak.bme.hu)>

## 5. OBJECTIVE

The objective of this benchmark is the detailed investigation of the velocity field in the flow straightener present in the BME 7 pin ALLEGRO rod bundle test section. The goal is the comparison of the participants' results to test the different CFD codes, models and code applications (used meshes, turbulence models, difference schemes, user effects, etc.). Since PIV experiments of the mentioned flow straightener have been carried out at BME, comparisons with experimental data to validate the CFD codes are possible.

## 6. INPUT

### 6.1. BOUNDARY CONDITIONS

The input data are coming from measurements of PIROUETTE test facility. The volumetric flow rate is set to 6 m<sup>3</sup>/h and is maintained under control thanks to the ultrasonic flow meters. The temperature of the water is 30°C and is maintained constant thanks to a heat exchanger, where at the second side there is mains tap water. Thanks to the heat exchanger, the model can be considered adiabatic in all its parts. The pressure of the water can be considered to be atmospheric at the outlet since the water is discharged in an open water tank. The properties of the water, such as density and dynamic viscosity, have to be computed considering the previously mentioned conditions, and the mass flow rate can be calculated considering these properties. The walls are considered smooth. The input data are summarized in Table 2. Regarding the physical walls, that include the straightener grids too, they are smooth and in no-slip condition. The flow in these conditions is turbulent both in the channels of the lamella that in the central part of the flow straightener:

$$Re_{centre} = \frac{4 \cdot \dot{m}}{\pi \cdot D_h \cdot \mu} = \frac{4 \cdot 1.6594}{\pi \cdot 0.05 \cdot 7.9735 \cdot 10^{-4}} = 52996 \quad (2)$$

$$Re_{channel} = \frac{4 \cdot \dot{m}}{\pi \cdot D_h \cdot \mu} = \frac{4 \cdot (1.6594 \div 25)}{\pi \cdot 8.4 \cdot 10^{-3} \cdot 7.9735 \cdot 10^{-4}} = 12618 \quad (3)$$

	Volumetric flow rate [m <sup>3</sup> /h]	Temperature [°C]	Pressure [bar]	Density [kg/m <sup>3</sup> ]	Dynamic viscosity [Pas]	Mass flow rate [kg/s]
Input value	6	30	1	995,6515	7,9735 E-4	1,6594

Table 2: Input data

### 6.2. GEOMETRY

In this section, details about the geometry can be found, in order to eliminate the errors that could come from a misunderstanding of the geometry and so from a wrong design. In Figure 6, the 3D CAD geometry of the flow straightener can be seen, while in **Chyba! Nenašiel sa žiaden zdroj odkazov.** some details regarding the grid's dimensions are given.

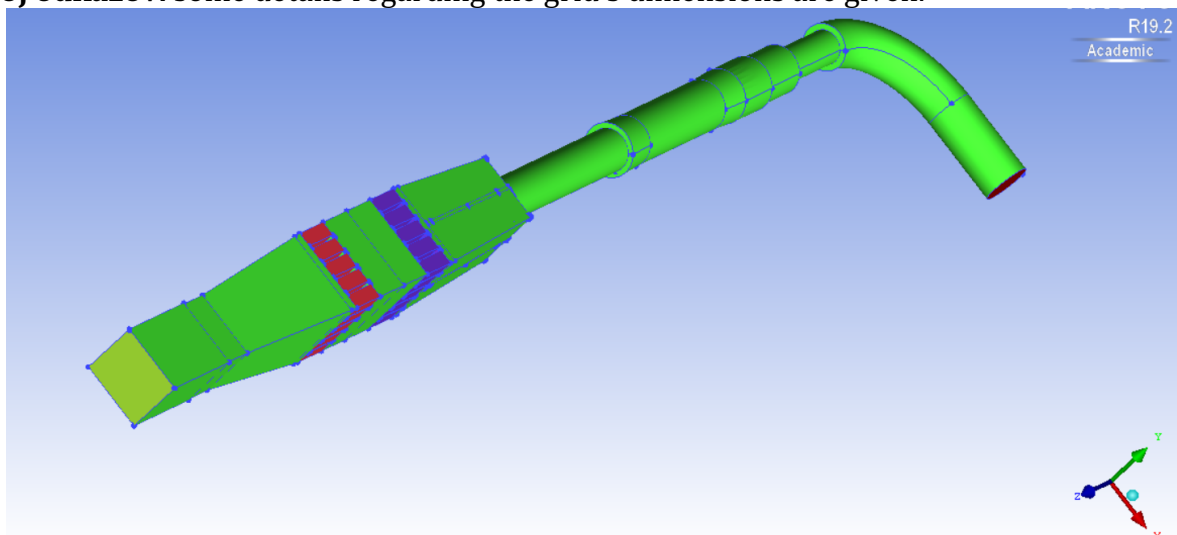


Figure 6: Geometry of the model in ICEM CFD

## 7. HARDWARE AND SOFTWARE REQUIREMENTS: MEMORY, FILES, APPROXIMATED COMPUTATIONAL TIME

Hardware requirements strongly depend on the complexity of the applied model (resolution of the mesh, used turbulence model etc.). For the calculations, a 3D CFD code (e.g. CFX, FLUENT, STAR CD, etc.) is needed.

## 8. OUTPUT

### 8.1. EXPECTED RESULTS

- Axial (W in Z direction) and transversal (U in X direction) velocity at each monitoring line shown in Figure 7 **Chyba! Nenašiel sa žiaden zdroj odkazov.** for each of the planes shown in Figure 4. The planes shown in Figure 4 are the same as shown in Figure 7. The Y=0 mm plane being the center one. The y positions of the planes in the flow straightener section are: -20.8mm; 0; 20.8 mm and at the beginning of the test section are: -10 mm, 0 mm and 10 mm. Regarding the monitoring lines, considering the delivered geometry file, in Table 3 are reported the points from where to where all the center lines of the evaluation are going, so that the comparison of the results is made easier. The same points can be used for the other planes changing the y-direction value.
- Model details: number of mesh nodes and elements, type of the mesh, turbulence model, boundary conditions, simulation type (steady state or transient), average value of Y+ (Yplus).
- It is important to note that the width of the monitor line is approximately 1,5 mm. For this reason, it is also recommended to perform the evaluation along a 1,5 mm wide strip (at the given Z height).

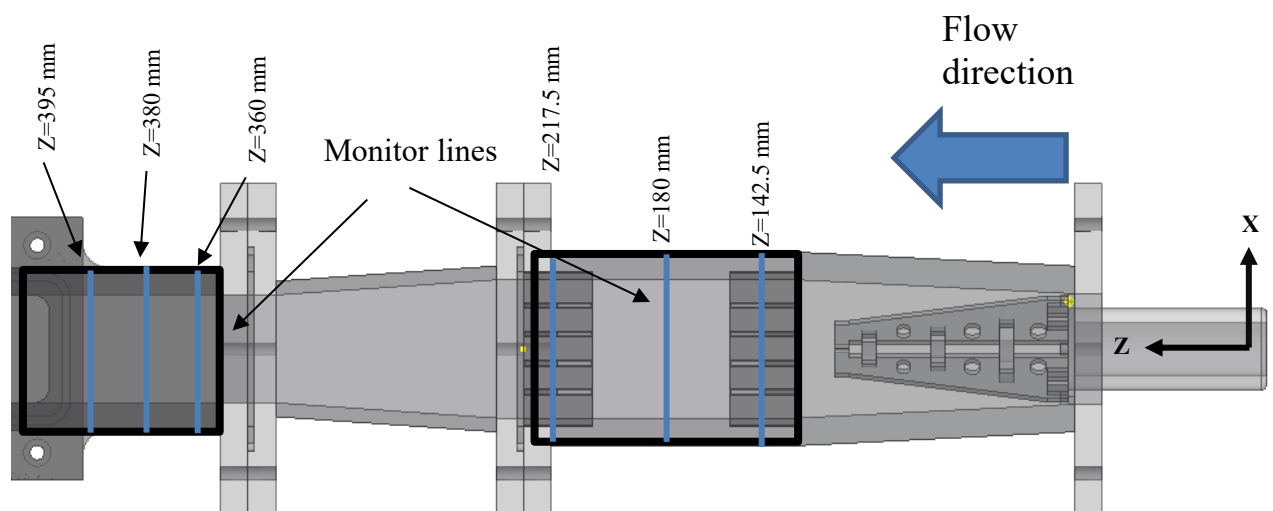


Figure 7. Monitor lines

	Starting point			Ending point		
	x	y	z	x	y	z
<b>Monitor lines inside the flow straightener</b>						
Y=0						
Z=142.5	-25	0	142.5	25	0	142.5
Z=180	-25	0	180	25	0	180
Z=217.5	-25	0	217.5	25	0	217.5
Y=-20.8						
Z=142.5	-25	-20.8	142.5	25	-20.8	142.5
Z=180	-25	-20.8	180	25	-20.8	180
Z=217.5	-25	-20.8	217.5	25	-20.8	217.5
Y=20.8						
Z=142.5	-25	20.8	142.5	25	20.8	142.5
Z=180	-25	20.8	180	25	20.8	180
Z=217.5	-25	20.8	217.5	25	20.8	217.5
<b>Monitor lines in the beginning of the measuring test section</b>						
Y=0						
Z=360	-20	0	360	20	0	360
Z=380	-20	0	380	20	0	380
Z=395	-20	0	395	20	0	395
Y=-10						
Z=360	-20	-10	360	20	-10	360
Z=380	-20	-10	380	20	-10	380
Z=395	-20	-10	395	20	-10	395
Y=10						
Z=360	-20	10	360	20	10	360
Z=380	-20	10	380	20	10	380
Z=390	-20	10	395	20	10	395

Table 3: Coordinates of the starting point and the ending point of the monitoring lines, all the dimensions are in [mm] (Coordinate axis are shown in Figure 4. 6.- and 7)

## 8.2. FILES FORMAT

The numerical data and the profiles are requested in MS Excel files.

The distributions should be printed in some kind of image files (e.g. \*.jpg, \*.png, \*.bmp).

Proposed dimensions: velocity [m/s].

## 9. OUTLOOK

Based on the experience gained during this benchmark a further benchmark exercise will be prepared in which the participants will investigate the flow field in a 7-rod bundle geometry with spacers relevant for ALLEGRO core geometries.

## REFERENCES

- [1] Data sheet: Economy MHIL 903,[Online], Available:  
<https://www.pumps.co.za/PageFiles/5155384441.pdf>.
- [2] Hydrus, DEIHL Metering, [Online], Available:  
<https://www.bellflowsystems.co.uk/files/attachments/5084/HYDRUS.pdf>.
- [3] D. Dynamics, Seeding particles for flow visualisation, LDA and PIV, Product information, Publication No.: Pi270003, 2002.
- [4] L. Lasers, Lamp Pumped lasers for PIV Applications from Litron, PB0101:3, 2010.
- [5] D. Dynamics, Light guide arm system, Publication No.: pi\_257\_v9, 2018.
- [6] V. Research, Phantom: Phantom Miro LAB/LC/R Series, ZDOC-64078-MA-0021 Rev 2, 2016.
- [7] D. Dynamics, Imaging Synchronization Devices, Product Information, Publication No.: pi:251\_v6, 2011.
- [8] D. Dynamics, DynamicStudio – User's Guide, Build no.: 6.9.0059. Publication no.: 9040U1871, 2019.
- [9] M. Raffel and co-aauthors, Particle Image Velocimetry - A practical guide, Springer, Berlin, Germany, 2007.
- [10] The Visualization Society of Japan, Handbook of Particle Image Velocimetry, Morikita Publishing, 2002, p. Chapter 6: Assessment and management of measurement accuracy.
- [11] B. Yamaji, Thermal-hydraulics of a homogeneous molten salt fast reactor concept – experimental and numerical analyses, PhD thesis, Budapest university of technology and economics, Institute of Nuclear Techniques, 2016.
- [12] AANSI ASME PTC, Measurement Uncertainty, Supplement of Instrument and Apparatus, Part 1, New York: ASME, 1986.
- [13] Z. Szatmáry, Mérések kiértékelése, egyetemi jegyzet, (Evaluation of measurements, lecture textbook), Budapest: BME TTK, 2010.
- [14] W. G. Steele, R. A. Ferguson, R. P. Taylor and H. W. Coleman, Comparison of ANSI/ASME and ISO models for calculation of uncertainty, ISA Transactions 33, 1994 (339-352).
- [15] M. Shao, *Technical Issues for Narrow Angle Astrometry (STEP)*, lecture note:  
[https://www.ias.tsinghua.edu.cn/\\_local/A/B5/87/B94081E75AB6CF53678D0DC3BEE\\_5AB93B48\\_191E66.pdf?e=.pdf](https://www.ias.tsinghua.edu.cn/_local/A/B5/87/B94081E75AB6CF53678D0DC3BEE_5AB93B48_191E66.pdf?e=.pdf), 2021.10.18.